School of Mechanical and Manufacturing Engineering

Faculty of Engineering

UNSW Sydney

Requirements to theses submitted in the Faculty of Engineering

by

Heidi Wright

Thesis submitted as a requirement for the degree of

Bachelor of Engineering in Mechanical Engineering

Submitted: May 2019 Student ID: z5016186

Supervisor: Dr. Susann Beier

ORIGINALITY STATEMENT

'I hereby declare that this submission is my own work and to the best of my knowledge it contains no materials previously published or written by another person, or substantial proportions of material which have been accepted for the award of any other degree or diploma at UNSW or any other educational institution, except where due acknowledgement is made in the thesis. Any contribution made to the research by others, with whom I have worked at UNSW or elsewhere, is explicitly acknowledged in the thesis. I also declare that the intellectual content of this thesis is the product of my own work, except to the extent that assistance from others in the project's design and conception or in style, presentation and linguistic expression is acknowledged.'

Signed 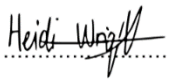

Date 30/5/2019

Abstract

Existing coronary artery stents continue to be subject to atherosclerosis, restenosis and stent thrombosis. These conditions have been linked to changes in hemodynamic factors involving wall shear stress (WSS), which can be influenced by stent geometry. Previous studies into stent design improvement have been largely restricted in the number of variables they consider to thoroughly understand their individual influence. This study aims to build upon this previous research concerned with design variables' influence on hemodynamic performance, addressing the need for comprehensive stent design improvement. Eight crucial design variables were identified (stent cross-sectional shape, stent width and height dimensions, strut angle, alignment type, distance between rings, connector type and number of connectors) and analysed for three objectives – low WSS, high WSS and time-averaged WSS.

In this study, the geometry of the stent is parameterised and a surrogate assisted multi-objective optimisation approach is used. Undesirable blood flow characteristics are minimised by suggesting improved stent parameters. From an initial sample set of 27 unique designs based on the eight variables, 10 non-dominated solutions are found. Updates using non sorted genetic algorithms (NSGA) and expected hypervolume improvement began to explore areas of uncertainty in the feasible objective space. Whilst further iterations are required for an optimal solution, the method is promising in achieving hemodynamically driven design improvements.

Acknowledgements

I would like to express my deep gratitude to Dr. Susann Beier in overseeing my thesis work, for her guidance, constructive critiques and assistance in accessing various resources. I would also like to thank Somesh Khullar, a fellow undergraduate engineering student, who spent months assisting in the development of the parameterised stent model. My grateful thanks also to thank Dr. Svetlana Tkachenko for her assistance in CFD modelling, and Dr Ray Taprabata for his expertise in multi-objective optimisation and assistance in processing data.

This research/project was undertaken with the assistance of resources and services from the National Computational Infrastructure (NCI), which is supported by the Australian Government. I would also like to extend thanks to the staff of the NCI for their timely and helpful responses to my requests for help.

.

Abbreviations

AT	Alignment Type
BE	Bachelor of Engineering
CAD	Computer Aided Design
CFD	Computational Fluid Dynamics
CA	Connector Arrangement
CH	Cell Height
CS	Cross Sectional Shape
CT	Connector Type
EHVI	Expected Hypervolume Improvement
EI	Expected Improvement
IA	Intra Strut Angle
ISR	In-Stent Restenosis
k	Turbulence kinetic energy
PCI	Percutaneous Coronary Intervention
SD1	Stent Dimension 1
SD2	Stent Dimension 2
ST	Stent Thrombosis
TAWSS	Time Averaged Wall Shear Stress
u	Velocity
WSS	Wall Shear Stress
ε	Rate of dissipation of turbulence energy
$\boldsymbol{\eta_i}$	Normal surface vector
ρ	Density
$\boldsymbol{\tau_{ij}}$	Viscous stress tensor

Contents

Abstract ..... **iii**

Acknowledgements ..... **iv**

Abbreviations ..... **v**

Contents ..... **vi**

List of Tables ..... **ix**

Chapter 1 Background **2**

1.1 Coronary Artery Disease 2

1.2 Treatment 2

1.3 Mechanisms of Failure 3

1.4 Role of Hemodynamic Studies in Failure Prevention 3

1.5 Computational Fluid Dynamic (CFD) Assessment of the Hemodynamic Environment 4

1.6 Limitations to CFD Modelling of Coronary Blood Flow 6

1.7 Opportunities for Hemodynamic Multi-Objective Optimisation 6

1.8 Background Summary 8

Chapter 2 Literature Review **9**

2.1 Important Design Variables 9

2.2 Computational Modelling of Coronary Flow 11

2.3 Optimisation of Stents 14

2.4 Research Motivation 18

Chapter 3 Method 19

3.1 Hemodynamic Objectives 19

3.2 Stent Geometry 20

3.3 CAD Modelling 24

3.4 CFD Environment 27

3.5 Multi-Objective Optimisation 29

Chapter 4 Results 33

4.1 Initial Sample Performance: Non-Dominated Set 34

4.2 NSGA Update 36

4.3 Expected Hypervolume Update 37

Chapter 5 Discussion 38

Conclusion 42

Bibliography 43

List of Figures

Figure 1. Percutaneous coronary intervention (PCI) 3
Figure 2. Types of stents available 3
Figure 3. Multi objective design space and feasible solutions 7
Figure 4. Stent Design Flow Chart 8
Figure 5. Diagram of Angle of Strut Alignment 10
Figure 6. Connector geometries analysed by Pant 11
Figure 7. Shear-Thinning Blood Behaviour 14
Figure 8. Optimisation process of stent design. 16
Figure 9. Stent Design Variables 20
Figure 10. Stent Dimensions for Strut Cross-Sections 21
Figure 11. Cell height lower boundary, 0.83mm, and upper boundary, 2mm. 22
Figure 12. Strut Alignment Types 22
Figure 13. Connector construction for i) straight, ii) spline, iii) semi-circular types 23
Figure 14. Number of connectors (NC), 1 per ring, 2 per ring, 1-2-1 alternating 23
Figure 15. Generation of Stented Artery Geometry 24
Figure 16. Mesh of stent i) cross-section, ii) longitudinal strut surface iii) whole stent. 25
Figure 17. Wall Shear Stress Visualisation of Varying Mesh Densities 26
Figure 18. Comparison of various meshes for WSS 26
Figure 19. Left main coronary blood flow over time 28
Figure 20. Flow chart detailing optimisation methodology 30
Figure 21. Sample stent designs. 31
Figure 22. Multi-objective performance of initial set of 27 samples 34
Figure 23. Two different views of the same multi-objective performance data 35
Figure 24. Truly evaluated non-dominated solutions and promising updates 35
Figure 25 WSS for 10 non-dominated solutions of the initial sample set. 36
Figure 26 Time averaged WSS for 10 non-dominated solutions of the initial sample set. 36
Figure 27. Expected hypervolume improvement solutions, left - solution 1, right, solution 2 37
Figure 28. Adverse TAWSS (%ge area) 39
Figure 29. Non-dominated solutions' range of design variables 40

List of Tables

Table 1. Review of Coronary Flow Modelling....12
Table 2. Comparison of stent design optimisation studies....15
Table 3. Summary of Design Variables and Boundaries....20
Table 4. Temporal Set-up....27
Table 5. Result matrix for all solutions, * non-dominated solutions....33
Table 6. NSGA updates....36

Thesis Overview

This study endeavours to consider the role of the geometric design variables of heart stents in shaping hemodynamic outcomes for patients. Much of the previous research in this area has concerned how singular design features characterise the blood flow changes around stents. This study details the formulation of an eight variable, multi-objective optimisation problem seeking to minimise adverse hemodynamic performance.

The project addresses two main deficiencies in current stent improvement research namely by 1) the inclusion of significantly more geometric variables (than previously considered in a single study) which have a role in altering the hemodynamic environment and, 2) the thorough consideration of multiple objectives which have been linked to undesirable patient outcomes.

Chapter 1

Background

1.1 Coronary Artery Disease

It is well known that coronary artery disease is the single most common cause of death worldwide [2, 3]. In Australia alone 645 000 people (3% of the population) self-reported instances of coronary artery disease in 2014-2015 [4]. Vascular injury causes cholesterol plaque to build up in the arteries (atherosclerosis), which can restrict the healthy flow of blood to the heart. The progression of the disease can involve the complete blockage of an artery causing death.

1.2 Treatment

Percutaneous coronary intervention (PCI) with stents is a common procedural response to the development of coronary artery disease. PCI involves the unclogging of closed (stenosed) coronary arteries with the aid of a small balloon insertion (*Figure 1 [5]*). Restenosis, the postprocedural reclosing of the artery, was a significant problem which necessitated repeat intervention in 30% of patients [6]. Elastic recoil of vascular tissue occurs in an inherent resistance to change shape. The efficacy of stenting instead of PCI alone to reduce restenosis rates was first reported by Sigwart et al. in 1987 and stents were approved and commercially available from 1994 [7]. Coronary stents have been heralded for their higher initial success rate, lesser invasiveness and long-term effectiveness in comparison to coronary artery bypass grafting or coronary balloon angioplasty.

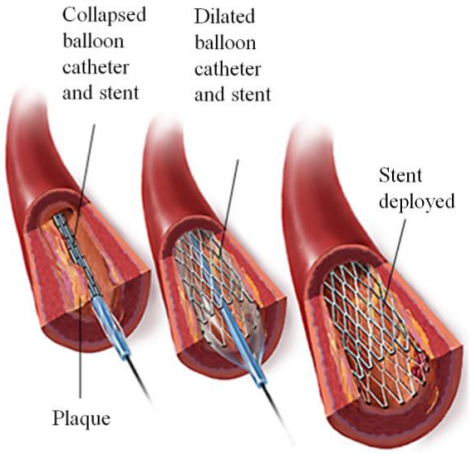

Figure 1. Percutaneous coronary intervention (PCI) where the collapsed balloon and stent are guided, with the catheter assistance, to the lesion (left), then the balloon is inflated to deploy the stent and compress the arterial plaque (middle), the balloon is subsequently removed leaving the deployed stent remaining (right). Adapted from [5].

Manufacturer	Image	Polymer/ Coating	Material	ST
1. BMS				
2. DES - Drug				
Abbott Vascular 1. Vision 2. Xience V - Everolimus		1.Nil 2.Durable	1.CoCr 2.L605	81
Medtronic 1. Integrity 2. Integrity Resolute - Zotarolimus	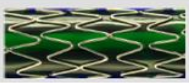	Durable	CoNi MP35N	81
Biosensors 1. No BMS 2. Biomatrix Flex - Biolimus A9	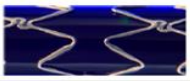	1.NA 2.Resorbable	316 SS	120
Boston Scientific 1. Omega 2a. Taxus Element - Paclitaxel / 2b. Promus Element - Everolimus	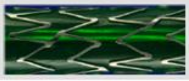	1. Durable 2. Durable	Pt Cr	81
Johnson & Johnson 1. Select 2. Cypher Select - Sirolimus		Durable	316 SS	140
Medtronic 1. Driver 2a. Endeavor / 2b. Endeavor Resolute - Zotarolimus		1. Durable 2. Durable	CoNi MP35N	91

BMS = bare-metal stent; DES = drug-eluting stent; ST = strut thickness in microns

Figure 2. Types of stents available

1.3 Mechanisms of Failure

Despite advances in stent technologies over the last 20 years PCI failure is still a relatively common occurrence. The development of stent design has been driven by increased understanding of their mechanisms of failure. In-stent restenosis (ISR) and stent thrombosis (ST) are the two key determinants of stent failure. Two percent of stent patients are dying due to thrombotic occlusion and fifteen percent require additional intervention for restenosis [2]. Numerous studies during the last decade have emphasised the previously underappreciated pivotal role of atherosclerosis in both ISR and ST [8, 9]. Many different commercial stent designs exist with no apparent 'best option' (*Figure 2*). Stent design determines hemodynamic changes in the vessel – changes which are a principal determinant in PCI outcomes [10]. Thus, consideration of stent design with respect to the hemodynamic changes the stent exerts on the vessel is key in reducing PCI failure.

Atherosclerosis is a condition where the arteries become narrowed and hardened due to accumulation of plaque around the artery wall.

In-stent restenosis (ISR) is defined as a reduction lumen diameter, or restenosis, of >50% in a previously stented segment.

Stent thrombosis (ST) is defined as the coagulation or clotting of blood in a previously stented segment.

1.4 Role of Hemodynamic Studies in Failure Prevention

Atherosclerosis in the coronaries is largely determined by the endothelial cell response. Flow disturbances have been hypothesised to be associated with changes in wall shear stress and endothelial function stimulation, which eventually leads to neointimal hyperplasia and restenosis [7]. The link between stent design and

restenosis, blood flow patterns and neointimal growth is well documented. Although the geometric design appears to largely contribute to the hemodynamic profile of the stented artery it is not well understood which design features may induce adverse blood flow changes, increasing the risk of clinical outcomes. Flow disturbance is characterised by wall shear stress. Wall shear stress (WSS) is the tangential drag force formed by blood flowing across the endothelial surface which regulates arterial wall remodelling. It is a function of the velocity gradient of blood nearest the endothelial surface. In the case of blood circulation there is a 'drag' induced between the outermost layer of blood in a vessel and the inner layer of vascular wall in contact with this blood.

Some well-established metrics can be considered to describe the effects of hemodynamic changes. These are high and low wall shear stress (WSS), and time averaged WSS (TAWSS).

Wall Shear Stress (WSS): Atheromatous disease locations frequently have relatively low WSS. At WSS < 1.5 Pa the release of tissue growth factors promotes intimal hyperplasia. Atherosclerotic intimal thickening is more prominent with lower WSS and areas with WSS < 0.5 Pa are predisposed to atherosclerosis (although this is of less danger to the patient as it is usually a stiffer and more stable plaque phenotype). Areas of coronary arteries with WSS > 1.2 Pa have been observed to have less atheromatous narrowing and more positive remodelling. In contrast it has been suggested that WSS > 2.5 Pa incubates development of a more vulnerable disease phenotype with plaques more vulnerable to rupture, which can lead to thrombus and occlusion. It is possible that both sites of low and high WSS carry increased risk of undesirable patient outcomes.

Time Averaged Wall Shear Stress (TAWSS): TAWSS is WSS averaged over the cardiac cycle to account for flow changes over time. Low TAWSS is associated with endothelialisation of stent struts, levels <0.5 Pa have been linked with cellular proliferation, intimal thickening, and inflammation.

1.5 Computational Fluid Dynamic (CFD) Assessment of the Hemodynamic Environment

Computational Fluid Dynamics (CFD) is a general term describing methods that seek the numerical solutions of the governing Navier-Stokes equations of fluid flow and has wide application across engineering disciplines [11]. CFD uses numerical methods to solve a set of governing partial differential equations which represent the laws of physics for prediction of velocity, pressure, stress and other variables. Relevant to this study, the Navier-Stokes equations of motion are considered which represent a force balance between pressure, acceleration, viscous and gravitational forces

$$\rho \frac{\partial u}{\partial t} + \rho(u.\nabla)u = \mu\nabla^2 u + f - \nabla p \tag{1.1}$$

Where u is the three-dimensional velocity field, f is a body force, p is the pressure field, ρ is the density of the fluid, and μ is the dynamic viscosity. Simplified for compressible fluids (such as blood)

$$\nabla . u = 0 \tag{1.2}$$

CFD modelling of arterial flow through stented vessels is of high importance in research as *in vivo* studies are often invasive, expensive and do not allow high resolution measurement in time and space. CFD facilitates design studies as input parameters and geometric variables can be easily altered to examine various scenarios of the simulation model. Continual advancements in computational power and resources allow computational studies to be adequately addressed.

The process of CFD analyses involve: i) building the virtual geometry of the stent, ii) discretization of the domain with a suitable mesh, iii) defining the physical model and its boundary conditions, iv) numerically solving the governing equations, v) post-processing the results for analysis, and vi) validation.

Stent Geometry: The virtual geometry of the stent is the domain of interest concerning coronary artery flow. In this case it is any prescribed stent design over a standard, idealized arterial segment.

Mesh Generation: The accuracy of the final solution is dependent on the quality of the mesh, how well the grid points are connected and located. The complicated geometry of a stented artery lends preference to unstructured meshes with fine grid size nearest the walls to best capture the fine detail of struts and solve for points of interest. There is a balancing act in achieving accurate and timely results as finer meshes improve accuracy but demand higher computational resources to solve.

Conditions: In order to mimic the arterial environment initial and boundary conditions must be applied to the system. Lack of knowledge and computational expense associated with exact replication of the arterial environment means simplifications are often made.

Solving and Analysis: Prior to analysis, the model is spatially and temporally discretised for accuracy and numerical stability of the solution. Mesh convergence identifies the suitable number of elements required to obtain a consistent solution whilst minimising exhaustive computational resource. Convergence and stability criteria are thereafter used to ensure results are numerically stable. Once the spatio-temporal resolution is satisfactory the results can be analysed for quantitative assessment, for example, blood induced wall shear stresses.

Validation: Results are validated against an acceptable standard which often involves comparison with either values measured within an in vitro phantom or acquired during *in vivo* assessment. This process enhances

confidence in the accuracy and reliability of the CFD model.

1.6 Limitations to CFD Modelling of Coronary Blood Flow

Numerical modelling relies on various simplifications and assumptions either because the problem is complex and finer details are not fully understood, computational limitations cannot handle the complexity of results or a converged solution cannot be achieved otherwise. Application of CFD to the study of arterial blood flows is significantly limited by uncertainties in defining the problem with requisite precision. Simulating coronary artery flow is challenging with respect to replicating tissue geometry and properties and boundary conditions being idealised. There is also limited understanding about numerous factors (pathophysiological, cell and structural). Obtained data on the hemodynamic environment cannot be readily verified by actual in vivo measurements due to simplifications in patient geometry and only represent approximations of actual values. However, although it is difficult to conclusively verify the relationship between stent design and the hemodynamic profile without in-vivo studies, computational fluid dynamics (CFD) can facilitate an understanding of these underlying issues.

1.7 Opportunities for Hemodynamic Multi-Objective Optimisation

Considerable research exists into which and how design variables influence coronary heart flow. There are multiple conditions which characterise undesirable coronary flow. In order to most effectively improve hemodynamic patient outcomes multiple objectives must be considered. A multi-objective optimisation problem (MOOP) involves more than one objective function that is to be minimised or maximised whereby the answer is a set of solutions that defines the best trade-off between competing objectives. The solution of a MOOP is determined by its dominance over any other given solution for the objectives sought. This is most easily visualised as a Pareto optimal solution. *Figure 3-a* depicts the feasible decision space, the designs possible for two variables, x_1 and x_2 and where their performance falls within the feasible objective space (*Figure 1-b)*. The Pareto-optimal set is the non-dominated set of the entire feasible decision space. The Pareto-optimal front describes the boundary where the objectives $f_1(x)$ and $f_2(x)$ are at their optimum plotted by the Pareto-optimum set. The overall goals in MOOP involve finding the set of solutions closest to the Pareto-optimal front and that the solutions be as diverse as possible.

Stent optimality has been examined throughout the literature and four key common elements resonate throughout; i) variable selection, ii) objective function definition, iii) constraint handling, and iv) the optimisation methods used.

Variable Selection: Control variables are the design or material parameters that may be accurately determined by designers and manufacturer and define the design space in which a deterministic solution is sought.

Objective Function Definition: The defining of the objectives sought can be done piecewise or formulated into a single objective.

Constraint Handling: Optimisation is often subject to complex constraints, commonly referred to as the 'bounds' of design variables, they act to define the design space of the problem. Most constraints imposed on stent optimisation studies are structural and are applied to the variables.

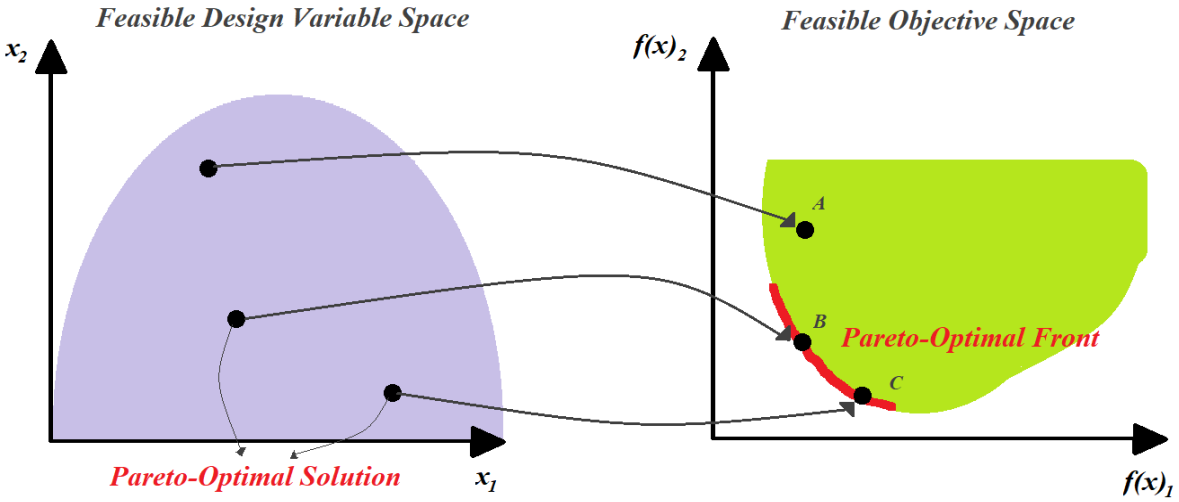

Figure 3. Multi objective design space and feasible solutions

Optimisation Methods: It would be infeasible to examine every design iteration possible for many variables thus surrogate modelling is commonly employed in order to reduce long computational times involved in simulation. Response surface models (RSMs) are constructed to interpolate the relationship between objective functions and design variables. In a MOOP, individual RSMs are constructed for each objective (and for each constraint in a constrained MOOP). Significantly, RSMs are only a prediction whose accuracy needs to be improved in order to determine an optimum. This improvement is achieved by generating new design point data at appropriate locations in the design space. Updates are made by searching the current RSM and running further simulation to obtain their objective outcomes. This process can be repeated until a convergence criterion is satisfied. It is suggested that ten times the number of design variables is an appropriate number of simulations to run. Validation of the quality of the RSM can be sought using cross-validation methods which sequentially compare predictions of at least one data point from RSMs constructed from the data set with these points excluded.

Kriging. Kriging has been the most widely used RSM optimisation method for heart stents. The Kriging model is regarded as a method of interpolation for spatial data. It considers the inputs, in this case the variables, and experimentally derived output data, the objectives, to observe spatial correlations. Usually, the result of kriging is the expected value ("kriging mean"), and the variance ("kriging variance") which is computed for every point within a region. The Kriging predictor i) contains a linear combination of tuneable

basis functions; ii) interpolates the data; iii) has a statistical interpretation from which the mean squared error (MSE) of the predictor can be formulated; iv) yields the expected improvement (EI), which can be used to enhance the search for optimal designs. Both the MSE and the EI are particularly useful for defining update points when it is necessary to improve the accuracy of the predictor. Kriging provides update points as the expected improvement (EI) function used repeatedly improves the accuracy of RSM in the design space and enhances the search for optimum designs.

1.8 Background Summary

Treatment of Coronary Artery Disease is often treated with PCI intervention and stent implant. There is a concerning rate of failure of these stents which can expose patients to undesirable risks including re-intervention or more seriously, death. This failure has been attributed to the adverse cellular responses triggered by alteration in coronary heart flow. The precursor to this is the stent geometry, of which there are many design variables, which alters the flow. Improving the arterial flow can be characterised by several objectives which seek to minimise blood-induced stresses (which can be analysed as a MOOP). Thus by considering the hemodynamic environment of the stent and how this is shaped by stent geometry, patient outcomes can be improved (Figure 4).

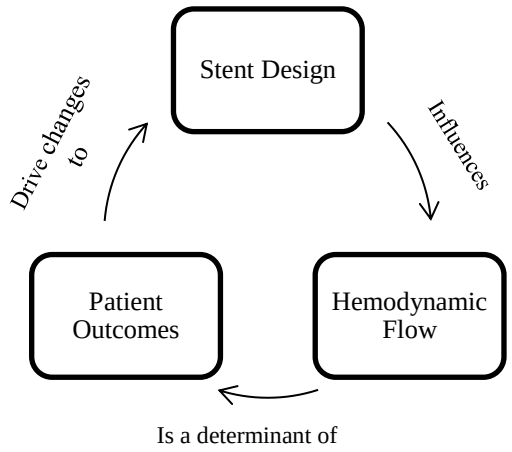

Figure 4. Stent Design Flow Chart

Chapter 2

Review of Coronary Flow Studies

This chapter provides a review of current data in relevance of design variables (Section 2.1) to hemodynamic outcomes (Section 2.2), followed by an overview of optimisation studies (Section 2.3). Finally, a brief summary is made concluding the contributions to the current work and how the present study seeks to address gaps in the literature (Section 2.4).

2.1 Important Design Variables

Numerous stent designs exist on the commercial market with significant variation in their geometries (REF FIG). The many variables are known to share complex relationships in shaping the performance of the stent, and hence patient outcomes. It is apparent that several design variables such as strut cross-sectional shape [12], stent connectors [13], strut alignment [14] and strut thickness [15] can influence coronary flow, the most crucial of these have been considered relevant in this study.

Cross Sectional Shape

Cross-sectional shape causes variations in hemodynamic flow, causing flow separation and recirculation zones. Slower moving fluid in a recirculation zone yields comparatively lower WSS which has been linked to retarding the endothelialisation process [16]. This condition can favour platelet aggregation and thrombogenesis. Typical cross-sectional shapes of stents have been ideally positioned triangular, rectangular or circular arcs of varying proportion [17]. It has been agreed upon in the literature that streamlined, and apposed stent struts cause less disruption to flow than non-streamlined, or malapposed stent struts [16-18]. It has also been shown that for square struts, the level of reverse flow correlates with the distance to the vessel wall whereas this effect is delayed spatially in circular struts [19]. A limitation of cross-sectional shape is the ability to achieve the precision manufacture of streamlined designs [12]. Thus, investigating both streamlined and non-streamlined struts would be of interest for the practical manufacture of optimised stents.

Strut Dimensions

Wall shear stress is very sensitive to strut thickness [15, 31]. A range of strut thicknesses are currently manufactured as seen in Fig 1. The smallest is the Supraflex™ 60µm [32] and thickness increases up to the Cypher™ at 140µm. Inter-strut spacing is important and should be large to re-establish interrupted flow [26]. Beier et al found that reduced strut spacing led to greater areas of adverse low WSS and high WSSG, but these effects were mitigated when strut size was reduced, particularly for WSSG [15]. The analysis by Gundert et al. of commercially realistic designs highlighted the benefits to favourable hemodynamic outcomes by minimising connectors and scaffolding to the minimum required to maintain similar initial strut thickness and stent to lumen ratios [33]. Putra et al. and Beier et al. both concluded that the adverse wall shear caused by thicker struts can be offset by increasing the cell height [20, 21]. Whilst smaller strut dimensions are beneficial for hemodynamic flow, they are also responsible for the high average stress on vessel surfaces owing to narrower contact surface area. Importantly, strut thickness is not an independent parameter and has been seen to interplay with other geometric modifications to alter hemodynamic flow.

Intra-Strut Angle

Strut alignment and the inter-strut angle has also been linked to alterations in hemodynamic flow [22]. The intra-strut angle involves the angle of the strut against the direction of flow (*Figure 5*). For a given ring of a specified cell height, a larger number of peaks naturally restricts the angle at each peak. Conversely, with a smaller number of peaks the angle is naturally inclined to be larger. Stent manufacturers produce stents of various sizes to accommodate for differing patient geometry.

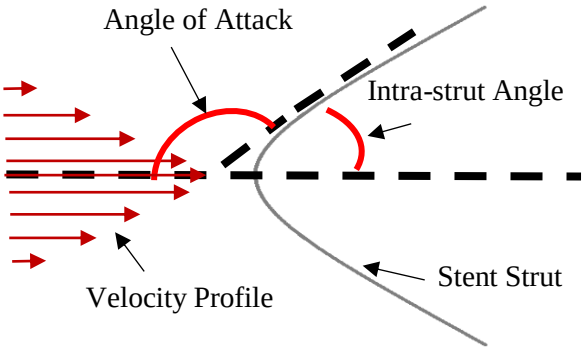

Figure 5. Diagram of Angle of Strut Alignment

Gundert et al. found that stent designs with an intra-strut angle of between approximately 38.5 deg and 46 deg minimized the area of low TAWSS apparently independent of vessel size or intra-strut area [23]. However, the author's later findings were conflicting, concluding that the intra strut angle may in fact be dependent on vessel size [14] This means the impact of the intra-strut angle on hemodynamic flow should be analysed with respect to factors which affect intra-strut area such as the alignment, strut thickness and connector geometry.

Alignment

The alignment of crowns in subsequent rings can vary. Typically, two configurations are observed; 'peak to peak' and 'peak to valley'. For example, Abbot Vascular's Vision stent is 'peak to peak' whereas Medtronic's Integrity is 'peak to valley'. Gundert et al. proposed that the alignment of the stent may also influence the ideal intra-strut angle [14, 24].

Cell Height

Cell height, the spacing between the rings of a strut, has been largely considered significant in shaping the hemodynamic arterial environment. In a simplified model of circumferential rings with varying spacing it was found that narrow cell height was the main cause of adverse WSSG across a pulsatile cycle and low WSS around peak flow [21]. Thus, it is apparent that cell height must be considered as narrower spacing reduces the intra-strut area and could significantly induce stress across the stent. Putra investigated cell height in triangular and rectangular stents and found the ideal cell height was also dependent on the strut cross-sectional shape [25]. It is apparent cell height is important but is also linked to strut size and shape.

Connector Geometry

Connectors link the rings of the strut and underpin the flexibility and strength of the design. In commercially available designs their geometry and positioning across the stent varies. From an idealised computational study up to 11% higher instantaneous WSS difference for a single strut spacing spanned by a connector versus no connector [26]. This highlights that connectors across the stent likely significantly induce stress. Pant considered a variety of connector geometries, *Figure 6*, finding that that cross-flow length and alignment with flow are key determinants of minimising blood flow disturbance [27]. To minimise instances of stress connectors would ideally be limited in number to the minimum required, of short crossflow length and aligned with the flow direction.

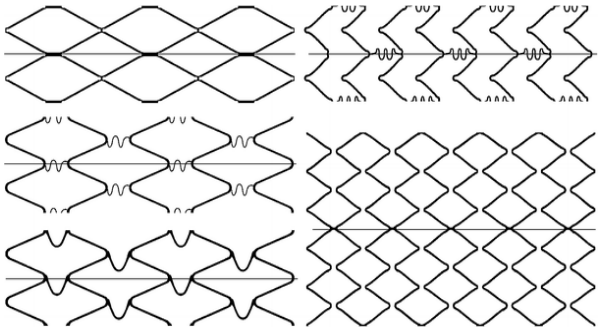

Figure 6. Connector geometries analysed by Pant

2.2 Computational Modelling of Coronary Flow

After the *in-silico* generation of the stented artery geometry, blood flow can be simulated in CFD. The discretisation of the blood flow is critical to accurately represent *in vivo* conditions. Numerous studies have sought to account for boundary conditions, blood behaviour, vessel compliance and motion. The following sections detail the most important aspects for CFD modelling. A summary of previous flow studies can be seen in *Table 1*.

Vessel Geometry The arterial environment is patient-specific, the curvature of the vessel and the presence of plaque is inherently difficult to simulate. Typically, an idealised artery is considered to overcome these issues whereby the vessel is cylindrical with constant diameter and the vessel wall is rigid. In reality most arteries have an approximately circular cross section but become narrower toward the periphery [28].

Table 1. Review of Coronary Flow Modelling

	Comprehensive Geometry	Deployment Deformation	3D	Pulsatile Flow	Non-Newtonian	Compliant	Motion
Poon et al. [19]	X	X	✔	✔	X	X	X
Gundert et al. [29]	✔	X	✔	✔	X	X	X
Hsiao et al. [15]	X	X	✔	✔	X	X	X
Gundert et al. [14]	✔	X	✔	✔	X	X	X
Gundert et al. [24]	✔	X	✔	✔	X	X	X
Pant et al. [30]	✔	X	✔	✔	X	X	X
Duraiswamy et al. [31]	X	X	✔	✔	X	X	X
Balossino et al. [33]	✔	✔	✔	✔	-	X	X
He et al. [26]	X	X	✔	✔	X	X	X
LaDisa et al. [34]	✔	X	✔	X	X	X	X
Beier et al. [21]	X	X	✔	✔	✔	X	X
Tammareddi et al. [35]	X	✔	✔	-	-	X	X
Pant et al. [27]	X	✔	✔	✔	X	X	X
Putra et al. [25]	X	✔	X	X	X	X	X

*Comprehensive geometry means idealised or patient-specific rather than simple/schematic; Deployment deformation means accounting for tissue prolapse; Compliant means an account of vessel compliance; Motion means modelling of cardiac/respiratory vessel motion. Note that ✔ represents an implemented feature, **X** not an implemented feature, and – information not provided.*

Mesh Generation To numerically analyse the stented artery the model is discretised into finite volumes. The selection of mesh type is dependent on the complexity of the topology. Stented arteries are inherently complex due to the protrusion of the stent struts into the flow. Often unstructured tetrahedral meshes have been used as they are quick and simple to generate, especially when many meshes are required [21, 36, 37]. Although good quality meshes can be produced, mesh convergence studies should be conducted to ensure the accuracy of the solution.

Boundary Conditions Following the creation of the fluid domain boundary conditions determine the qualification of the conceptual model as a replication of the actual arterial environment. This commonly comprises of the inlet velocity profile, pulsatile description of the cardiac cycle and outlet conditions.

Inlet Profile The velocity profile over a given vessel cross section is not uniform as the velocity at the centre of the vessel is higher than at the walls. Studies which have assumed uniformity over the cross-section introduces errors in the first few diameters of the inlet, after which the flow will be fully developed. An elongation of the inlet length prior to the stent can remove these inlet effects on the computed flow field an ensure a fully developed velocity profile in the entry region [21].

Pulsatile Flow The pumping action of the cardiac cycle causes rapid and significant change in flow, velocity and pressure through the coronaries. To comprehensively understand the hemodynamic changes, a time dependent analyses is preferred [38]. Intra-coronary transducers have been used previously to obtain pressure and Doppler velocity information [39]. This has since been used to prescribe inlet conditions in computational studies [21, 37]. More recently it has been contested by Putra et al. that there is negligible difference in prescribing pulsatile versus steady flow, however this could be due to further simplifications made such as Newtonian flow which may have eroded the accuracy of near-wall results [20, 25]. Including pulsatile flow would be suggested to more closely replicate the actual arterial environment.

Outlet Profile The two common practises to define the outlet boundary conditions are either constant pressure or, in the case of a bifurcated artery, to define split flow ratio to the daughter branches. The outlet should also be extended to observe any downstream flow behaviour [21]. Most commonly in design improvement studies, a constant pressure outlet is prescribed [21, 27, 32, 33].

Blood Rheology Non-Newtonian flow behaviour should be accounted for in any CFD modelling. For reasons of simplicity many studies have considered blood as Newtonian with a constant value viscosity. This severely limits the accuracy of WSS as blood only behaves as a Newtonian fluid for shear rates above $100s^{-1}$, in lower shear rates the viscosity decreases exponentially with decreasing shear [39]. This is especially evident in pulsatile simulations where Newtonian models consistently yield lower WSS values across the entire cardiac cycle [40]. Blood, however, should be considered as non-Newtonian as the dynamic viscosity depends on shear rate. This is because blood includes a suspension of sizeable particles such as erythrocytes, leukocytes, and platelets in blood plasma. At low shear rates the apparent viscosity increases and at higher shear rates the apparent viscosity is dependent on vessel size, the viscosity smaller in small vessels and higher in large vessels [39]*(Figure 7)*. The ‘Carreau-Yasuda’ model has been found to be the most accurate to describe the non-Newtonian behaviour of blood.

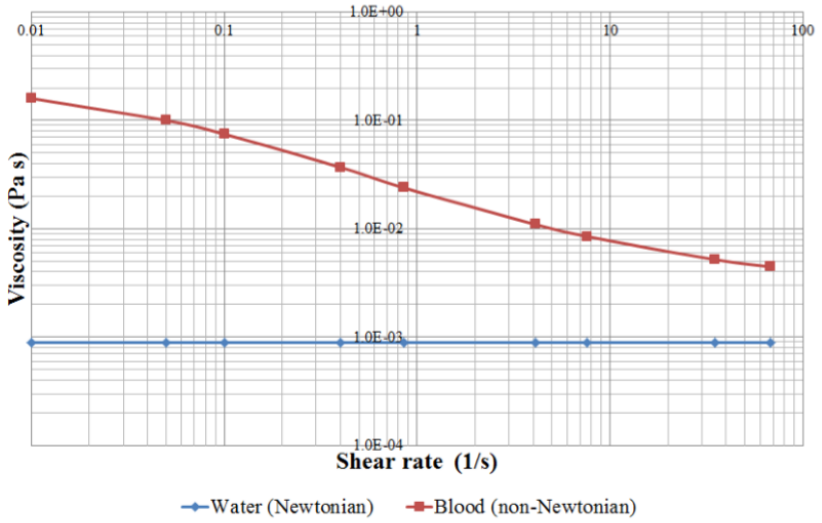

Figure 7. Shear-Thinning Blood Behaviour - Dynamic viscosity over shear rate shown for water at 25◦C (Newtonian behaviour) versus blood (non-Newtonian shear-thinning fluid properties) [1]

Vessel Compliance There is uncertainty about arterial vessel properties and a few studies have sought to quantify the difference in rigid models versus fluid-structure interaction (FSI) models. The realistic anisotropic properties of vessels are unknown but in previous research attempting to quantify the difference in rigid and FSI models it was found that the discrepancies in hemodynamic differences were minor [41]. In the only conflicting study, flow measurements in straight, elastic tubes showed up to 30% difference in time averaged WSS and WSS. However, the extent to which an elastic tube represents a coronary artery wall is still unconfirmed. Previous studies have often simplified the coronaries to being rigid and without motion based on these findings, and by virtue of lower computational cost.

2.3 Optimisation of Stents

After a computational model is generated, blood flow can be simulated through the relevant designs and analysed for desired objectives *Figure 8*. The optimisation of design variables for a singular or multiple objective has been seen throughout the literature (*Table 2*). The solutions of each study were representative of these variables and objectives considered. As discussed previously, there are many variables which share a complex relationship and have been connected to adverse hemodynamic outcomes. Whilst considering design variables piecewise is useful in initially understanding how each design feature contributes to altered flow, upon this base knowledge more global design improvement can be made.

Table 2. Comparison of stent design optimisation studies

Author	Focus	Objective(s)	Geometry	Contributions	Limitations	Optimisation Method
Pant et al. [27]	Whole stent	i) acute recoil, ii) tissue stresses, iii) haemodynamic disturbance, iv) drug delivery v) uniformity of drug supply, vi) flexibility	Straight, idealised	Several optimal designs achieved for various trade-offs.	Newtonian fluid model.	Kriging with NGSA-II
Gundert et al. (2013) [29]	Whole stent	Velocity, mean exposure time, and distributions of WSS.	Straight, idealised	Number of struts and connectors should be minimised for structural necessity.	Inconclusive in terms of recommendations as similar designs were studied.	No optimisation, quantitative comparison of different stent designs.
Gundert et al. (2012) [14]	Whole stent	Minimise time averaged WSS.	Straight, idealised	Alignment seemed important; number of crowns should be minimised to necessity.	Too many features were changed, not enough controlled variables, limiting conclusive results.	Cost function to minimise time averaged WSS disturbance
Gundert et al. [24] (2012)	Whole stent	i) number of crowns, ii) intra-strut angle	Straight, idealised	Ideal crown number dependent on diameter	Contradiction to own previous studies.	Cost function to minimise time averaged WSS disturbance
Beier et al. [21]	Whole stent	i) low WSS, ii) high WSS, iii) time averaged WSS, iv) WSS gradient.	Straight, idealised (4mm)	Strut spacing, thickness, luminal protrusion and alignment were important.		Piecewise for each variable
Tammaredi et al. [35]	Whole Stent	i) Average arterial stress (deployment), ii) Elastic recoil (balloon deflation)	Straight, three arterial layers	More robust solution by accounting for many uncertainties, but no optimal solution found.	Stress only considered for deployment and deflation, not blood flow.	Multi-objective Particle Swarm Optimization (MOPSO) algorithm
Putra et al. (2017) [20]	Steady and Pulsatile Flow	Compare steady and pulsatile flow.	Straight, idealised	Difference in using steady or pulsatile flow is insignificant.	Singular objective, reducing low WSS, did not consider a time averaged approach and Newtonian fluid model.	Kriging with EI: error-based exploitation (EBE) method
Putra et al. (2018)	i) cell height, ii) length and iii) strut cross-sectional size for triangular and square stents	Minimise average stress and low wall shear stress ratio	Straight, idealised (4mm)	Triangular stent preferential. Cell height and strut dimensions have shared impact of WSS.	Used Newtonian fluid model.	Kriging method and expected hypervolume improvement (EHVI)

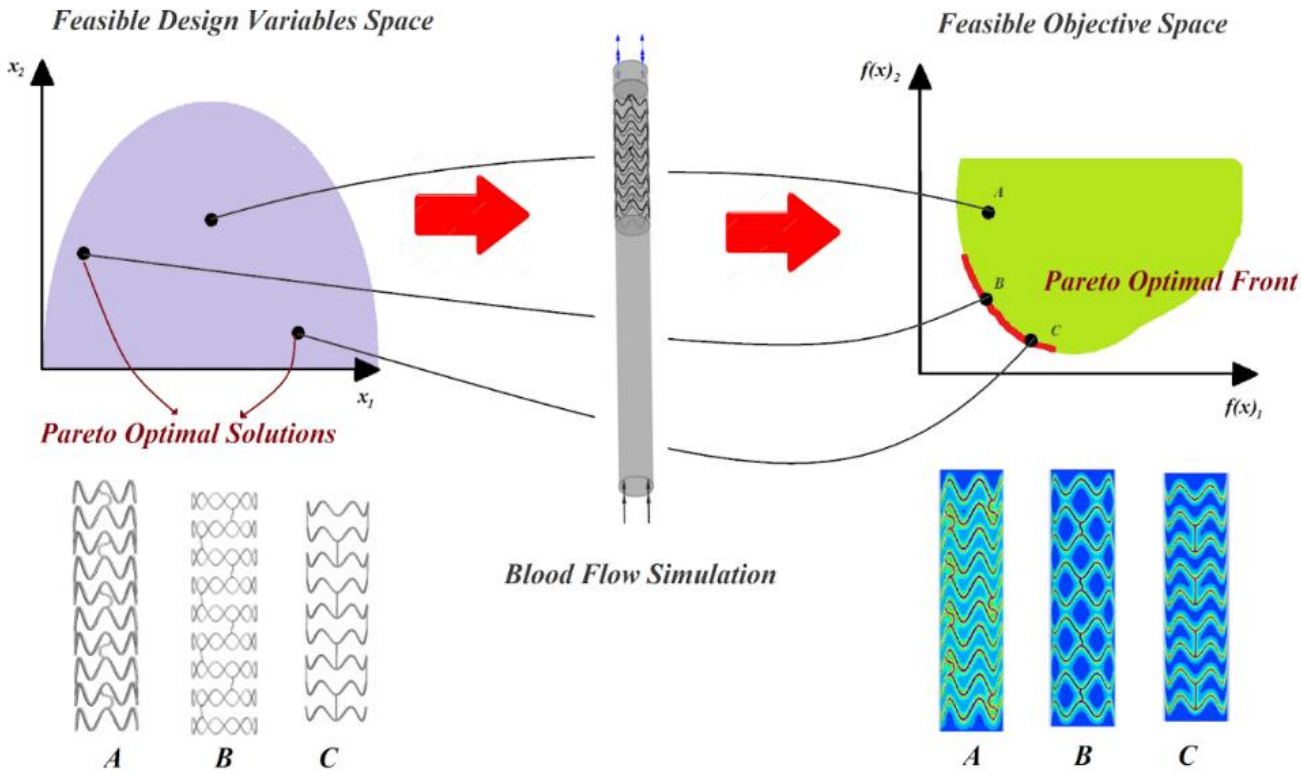

Figure 8. Optimisation process of stent design – Designs are generated within the feasible design space and then blood flow is simulated in order to assess the design's performance for the desired objective/s.

Variable Selection In previous stent MOOPs, typically only three or four variables have been considered [25, 35] except for Grogan et al. and Wu et al [42, 43]. Strut width and thickness is the most prominently included variable, strut length and parameters to control peak shape are also common. In studies specific to hemodynamic objectives Beier et al. considered strut spacing and wall protrusion and Atherton & Bates and Gundert et al. the intra-strut angle was included [24, 44].

Hemodynamic Objectives Minimising low WSS has typically been the primary hemodynamic objective across the literature. Pant et al. considered the interplay of ring height, strut width and connector height to optimise stent design for six objective outcomes. Among these objectives an index for hemodynamic low and reverse flow was used to quantify the relevant flow features concerning stented-vessel hemodynamics into one numeric quantity. Putra tailored their objectives to low WSS and stress inflicted on the surface but modelling as a steady-state meant the time-averaged effects were missed[25]. In both Pant et al. and Putra et al. hemodynamic factors were simplified and overlooked higher values of WSS or how WSS changed over space and time which has also been linked to adverse patient outcomes (Section 1.4 Role of Hemodynamic Studies in Failure Prevention). Importantly, Beier et al. thoroughly engaged with hemodynamics considering the three most established metrics, WSS, TAWSS and WSSG. The author examined design variables (strut spacing, strut size, cell height and strut protrusion) individually to examine their effects on the hemodynamic

environment.

Objective Function Definition For MOOPs, studies have often attempted to reconcile to a single weighted objective function [45-47] however these studies were convex and had no variables were constrained to be integers. In order to examine variables such as alignment which are non-convex interval values of 0° or 180°, non-dominated solutions cannot be found using the weighted method. Increasingly sophisticated endeavours have been made to search Pareto fronts treating objectives separately [48], and the use of non-dominated genetic sorting algorithm, NGSA II has been adopted by Pant et al. [27] for six objectives and Clune et al [49] for a fracture resistance and flexibility trade-off.

Constraints Most constraints imposed on stent optimisation studies are structural and are applied to the variables. Few studies have directly constrained objectives such as Bozsak et al. who sought to keep eluting drug concentrations away from toxic levels by introducing a term to penalise the objective function [47].

Optimisation and Improvement Methods The method of improving the optimisation has varied through the literature. EI has been conventionally used as the criterion considering the stochastic improvement of each objective function value individually in general optimisation problems. The success of Kriging with EI lead Li et al. [43] to achieve designs with reduced dog-boning. This singular-objective optimisation used simplified geometry for four variables with the maximum number of updates being 22.

Notably, Pant et al. (2011) constructed individual Krigs for six separate objectives were used in a non-dominated sorting genetic algorithm, NSGA II, search of the design space. A total of 30 evaluations were considered for the three variables - divided into an initial sampling of 15 points, and three subsequent updates, each update adding five new points. This successfully brought them to optimise for six objectives as a family of non-dominated solutions.

Kriging with expected hypervolume improvement (EHVI) was used by Putra et al. to minimise average stress and low wall shear stress ratio for cell height, length and strut cross-sectional size for triangular and square stents [25]. The literature suggests that EHVI can has greater advantage of convergence and diversity to the true Pareto-optimal over EST and EI as the number of objective functions increases [50]. Conflictingly, the same author observed EHVI showing a slower convergence to the true Pareto-optimal front. The success of the improvement method is dependent on the complexity of the objective function space [50].

In summary of the studies concerned with improving the hemodynamic environment, many have prioritised minimising low WSS. Beier et al. provided the most comprehensive framework for analysing the hemodynamic environment with four key objectives. Most optimisation studies have only considered three or four design variables although there is evidence that there is a wider selection which may influence the

hemodynamic environment. This represents a gap of knowledge considering the complex interaction of many variables and how they can be optimised for several hemodynamic outcomes. In terms of MOOP method, Kriging has been widely used across stent optimisation problems but as for improvement and updating strategies there is no clear best practise.

2.4 Research Motivation

The hemodynamic environment of the stented artery, which can manipulate patient outcomes, is determined by the geometric design of the stent. Upon review of the literature it is apparent that there are many geometric variables which can alter blood flow. Furthermore, to effectively consider changes to the hemodynamic environment, several measures of wall shear stress can be considered as undesirable for patient outcomes. Stent design improvement studies have often only focussed on three or four design variables and shallowly considered undesirable hemodynamic performance. This represents a gap of knowledge considering the complex interaction of many variables and how they can be optimised for several hemodynamic outcomes. A solution to a design improvement problem is as only good as the design space and objectives considered. Therefore, the purpose of this research is to more thoroughly understand how many design variables influence the hemodynamic environment, for multiple objectives.

Chapter 3

Method

The aim of this study is to identify optimal stent design characteristics in consideration of multiple hemodynamic objectives. This investigation will be an extension of the work of Beier et al. modifying the parameters chosen and extending the line of inquiry to involve a more comprehensive multi-objective output. This chapter outlines the generation of stent geometry, definition of the CFD environment and process of multi-objective optimisation.

3.1 Hemodynamic Objectives

The stent is to be optimised to minimise disruption to the coronary flow, characterised by wall shear stress over space and time. The WSS vector describes the flow-induced viscous forces exerted on luminal and stent surfaces such that,

$$|WSS| = |\eta_i . \tau_{ij}|$$

Where η_i denotes the surface normal vector, and τ_{ij}, denotes the viscous stress tensor. Newtonian fluids by definition have constant dynamic viscosity at all rates of shear [39]. It is possible that both sites of low and high WSS carry increased risk of undesirable patient outcomes.

Low Wall Shear Stress (LWSS): Total percentage surface area of WSS <0.5 Pa is to be minimised as they are areas predisposed to atherosclerosis.

High Wall Shear Stress (HWSS): Total percentage surface area of WSS > 2.5 Pa is to be minimised as these areas have been associated with the development of plaques more vulnerable to rupture, which can lead to thrombus and occlusion.

Time Averaged Wall Shear Stress (TAWSS): WSS averaged over the cardiac cycle to

account for flow changes over time. Total percentage surface area of TAWSS <0.5Pa is to be minimised as these areas have been linked with cellular proliferation, intimal thickening, and inflammation.

3.2 Stent Geometry

The stent geometry was generated to reflect the design variables in a parameterised CAD model. WSS is inversely proportional to the cube of the radius, small changes in vessel size would strongly alter the WSS profile. Therefore, for analyses of wall shear stress, the vessel size is kept constant at 3mm to determine the effect of other variables.

3.2.1 Design Variables

Eight significant design variables were considered in the stent geometry (*Figure 9*); i) cross-sectional shape, ii) strut dimension 1, iii) strut dimension 2, iv) intra-strut angle, v) alignment type, vi) cell height, vii) connector type, viii) connector arrangement. A summary of the bounds of each variable are in *Table 3*.

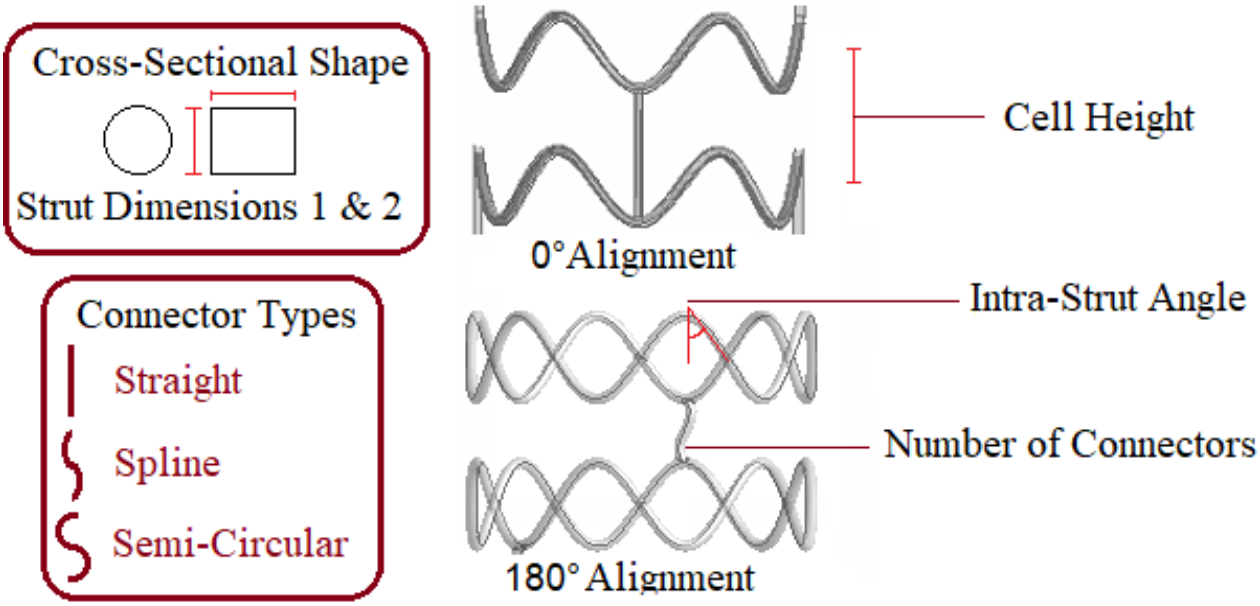

Figure 9. Stent Design Variables

Table 3 Summary of Design Variables and Boundaries

Variable	Boundary Summary
Cross Sectional Shape	1 = Rectangular 2 = Circular
Strut Dimension 1	Lower Bound: 60 µm
	Upper Bound: 120 µm
Strut Dimension 2	Lower Bound: 60 µm
	Upper Bound: 120 µm

Intra-Strut Angle	Lower Bound: 25°
	Upper Bound: 50°
Alignment Type	0° or 180°
Cell Height	Lower Bound: 0.83mm
	Upper Bound: 2mm
Connector Type	1 = Straight Line 2 = Spline 3 = Semi-Circular
Number of Connectors	1 = One/ring 2 = Two/ring 3 = Alternating 1-2-1

Cross Sectional Shape (CS): Rectangular (CS1) and circular (CS2) strut cross-sections are to be examined (*Figure 10*), optimal design for both shapes is sought.

Strut Dimensions (SD1, SD2): Two dimensions are to account for the cross-sectional strut geometry accounting for both circular and rectangular shapes. SD1 is indicative of the width of a rectangular strut or the diameter of a circular strut whereas SD2 will only apply to the height of a rectangular strut. The lower bound is 60µm, the upper bound is 120µm to reflect commercially available designs [REF].

Strut Cross-Section	**SD1**	**SD2**
Circular	Diameter	-
Rectangular	Width	Height

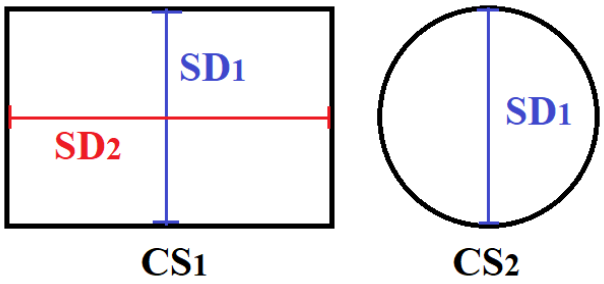

Figure 10. Stent Dimensions for Strut Cross-Sections

Intra-Strut Angle (IA): The intra-strut angle is restricted within the bounds of cell height and the six-peak configuration to be examined. The lower bound is 25°, the upper bound is 50°.

Alignment Type (AT): Two alignments of 0°, or ‘peak-to-peak’, and 180°, or ‘peak-to-trough’ were considered (*Figure 12*).

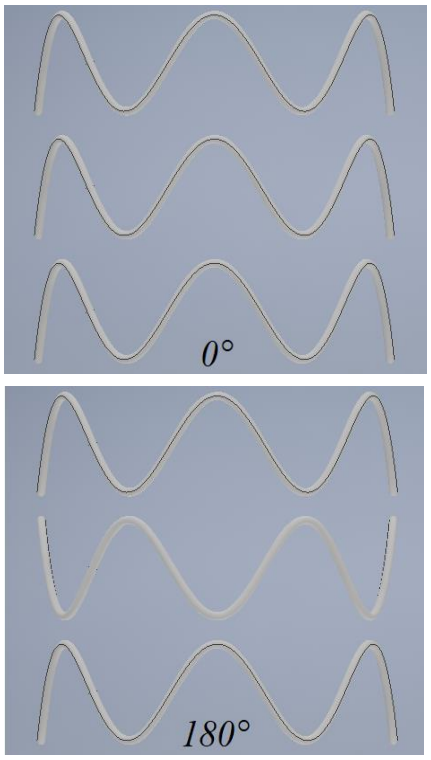

Figure 12. Strut Alignment Types

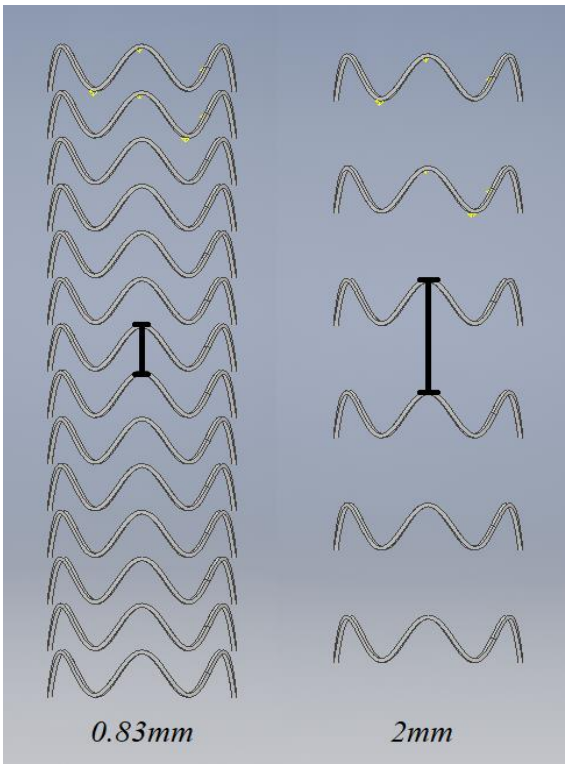

Figure 11. Cell height lower boundary, 0.83mm, and upper boundary, 2mm.

Cell Height (CH): Cell height, the spacing between the rings of a strut, has been largely considered significant in shaping the hemodynamic arterial environment [24]. The bounds of the cell height reflect the work of Beier et al. [21] with an upper bound of *2mm* and a lower bound of *0.83mm* (*Figure 11*). The upper bound of *CH* is chosen considering that very high values will result in little structural support between rings. The lower bound of *CH* is chosen considering that very low values will result in contact of one ring with another with respect to the *SA* chosen.

The stent length is a maximum of *12mm* and the diameter is *3mm*. The number of rings is dependent on the cell height such that,

$$NR = ceil(\frac{11}{10 * CH})$$

Connector Type (CT): Three connector types considered: straight line, spline and semi-circular. 3D Construction points are generated on the base geometry formulated by the IA, AT and CH and CT (*Figure 13*) and then swept for the applicable strut dimensions along the curve.

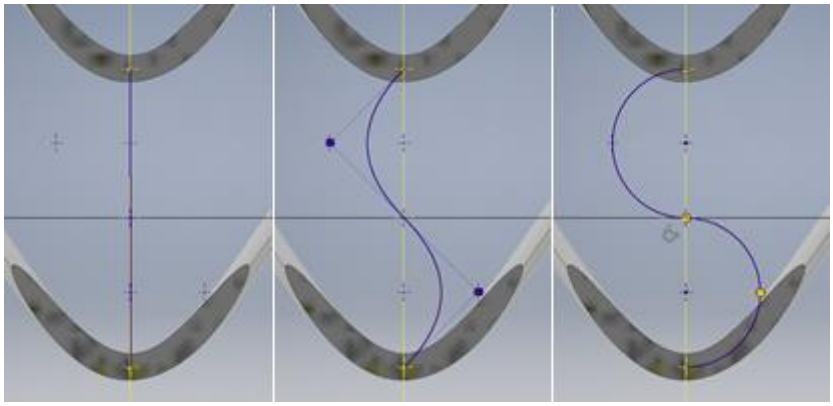

Figure 13. Connector construction for i) straight, ii) spline, iii) semi-circular types

Connector Arrangement (CA): Three configurations of connector arrangements were considered, i) one per ring, ii) two per ring, iii) 1-2-1 alternating (*Figure 14*).

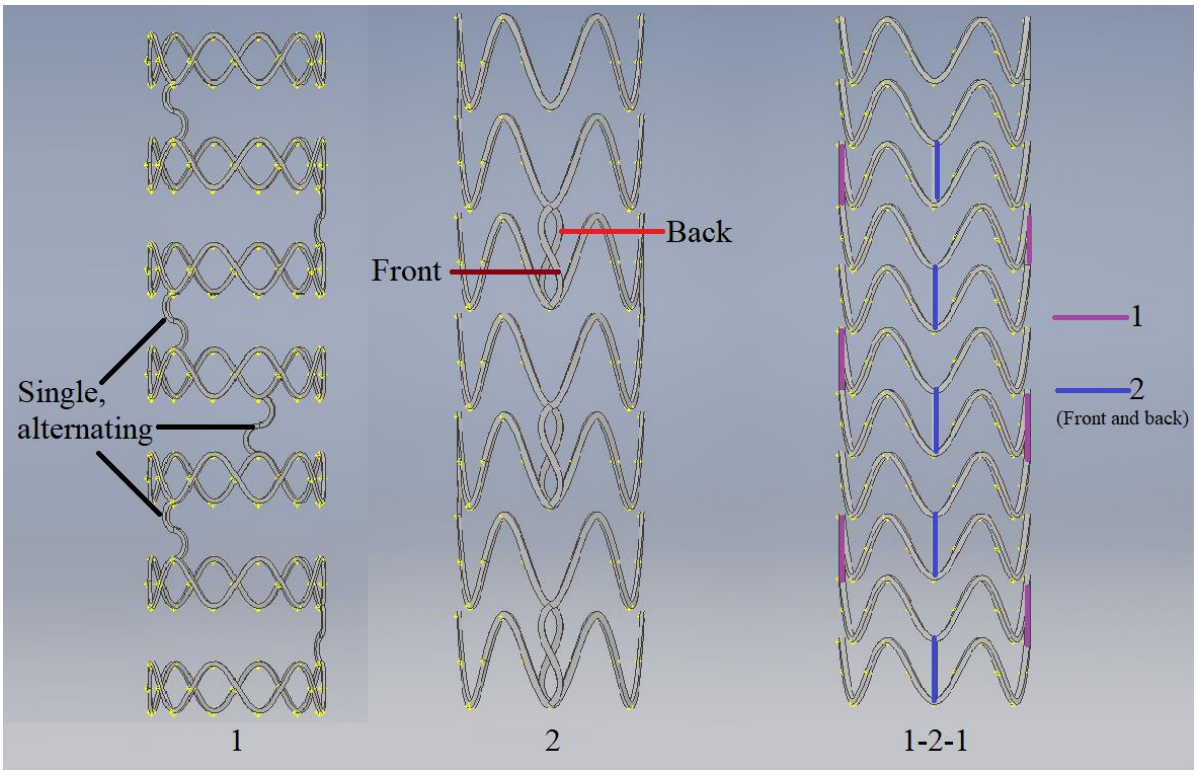

Figure 14. Number of connectors (NC), 1 per ring, 2 per ring, 1-2-1 alternating

3.3 CAD Modelling

A parameterised CAD model was generated to account for the eight design variables. The CAD models do not represent any singular commercially available stent, rather they are amalgamations of the identified, most crucial design variables. Initially a base ring layer was created. To simplify the number of variables the ring geometry was projected along a sinusoidal wave, approximated using the intra-strut angle (SA), number of peaks (s*ix*), and stent diameter (*3mm*).

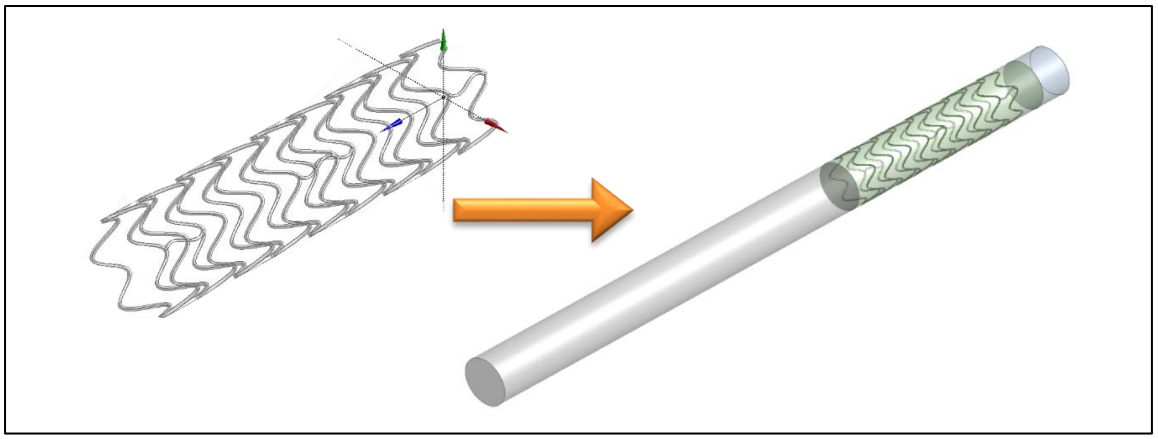

Figure 15. Generation of Stented Artery Geometry

Points were then generated as a 3D sketch dependent on the base ring geometry, the type of connector and number of connectors. Depending on the type of connector a shape is drawn between these points and swept and patterned as necessary. Intersecting geometry is trimmed to the ring. The entrance is extended to account for full development of flow and the negative volume of the combined structure is taken for modelling. The simulated arterial environment is idealised in a straight tubular geometry of 50% stent apposition into the vessel wall using a primitive cylinder and a Boolean subtraction operation *(Figure 15*).

High Performance Computing

This project was undertaken with the assistance of resources and services from the National Computational Infrastructure (NCI), which is supported by the Australian Government.

3.3.1 Mesh Generation

A patch-conforming, unstructured tetrahedral mesh with variable mesh spacing was created in ANSYS 19.1. Increased mesh density was present along strut faces, to account for complex geometry, and expected hemodynamic disturbance (*Figure 16*) whereas a relatively coarse mesh was applied in the unstented region.

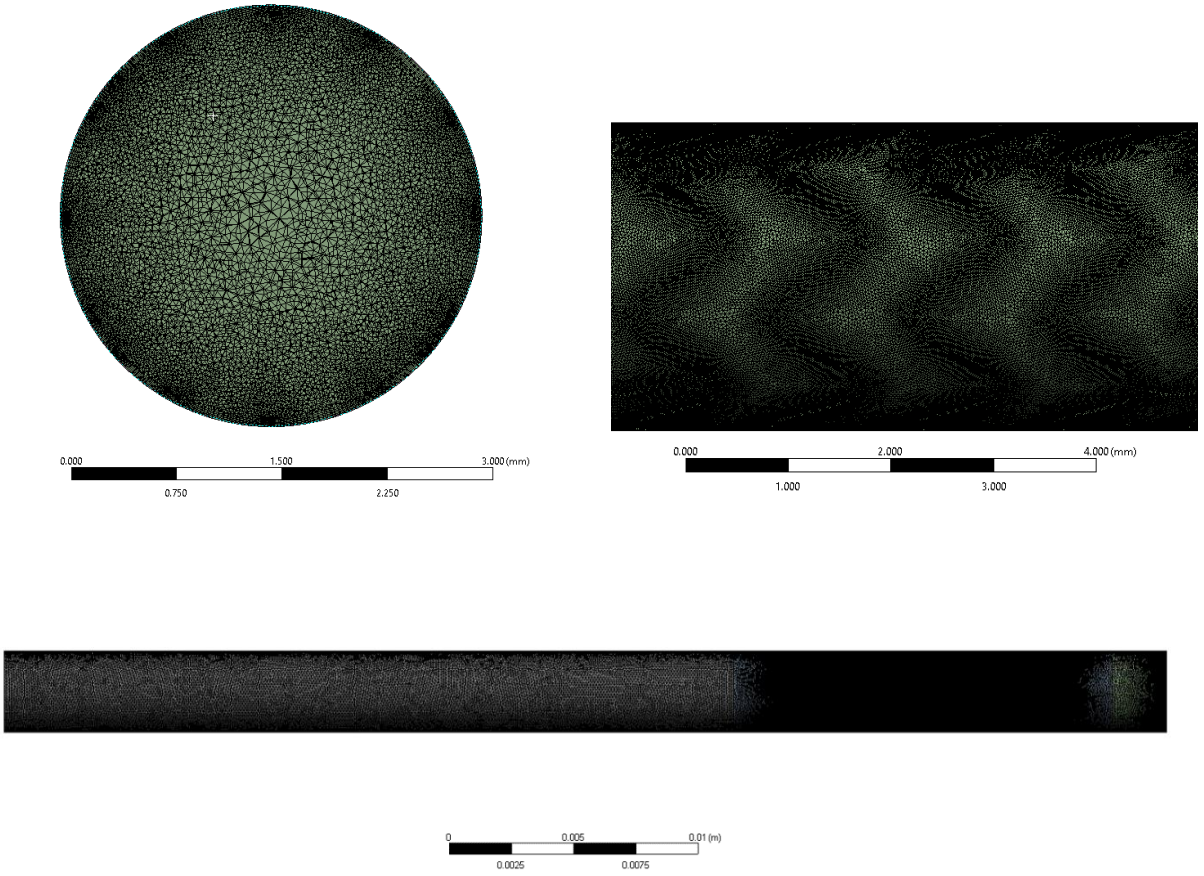

Figure 16. Mesh of stent i) cross-section, ii) longitudinal strut surface iii) whole stent with extended inlet and outlet, more detail present around strut surface.

3.3.2 Mesh Sensitivity Study

A mesh sensitivity study was undertaken to determine the mesh most suitable to providing accurate hemodynamic behaviour within reasonable computational load. Increasing mesh density meant more accurate representation of the location and magnitude of stresses present, as observed by the higher definition of colour transition in *Figure 17*. Importantly, it was not feasible to verify the CFD results of every single stent model as independent of mesh density as only one mesh was created per model. Creating multiple meshes to ensure mesh-independence of each model was infeasible due to time constraints for the project. From the mesh sensitivity study performed at minimum 16 million element meshes were used, with upward of 20 million elements for more complex stents with spline or semi-circular connectors.

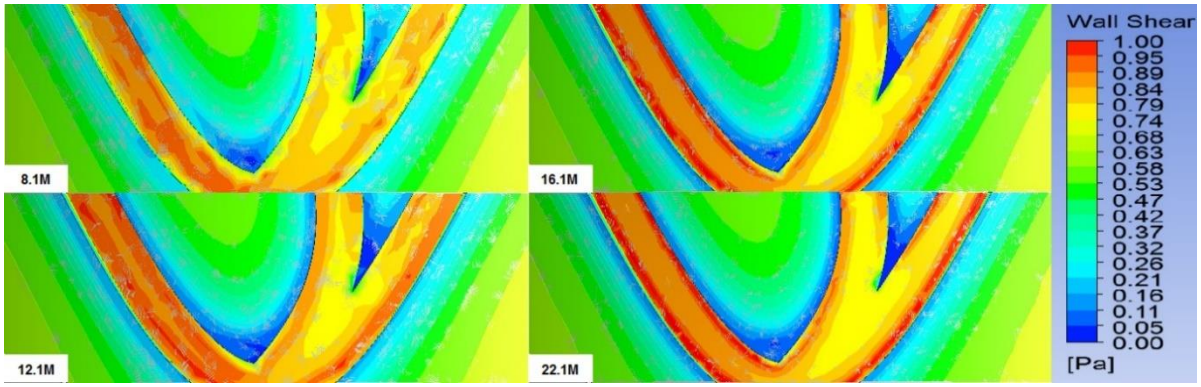

Figure 17. Wall Shear Stress Visualisation of Varying Mesh Densities

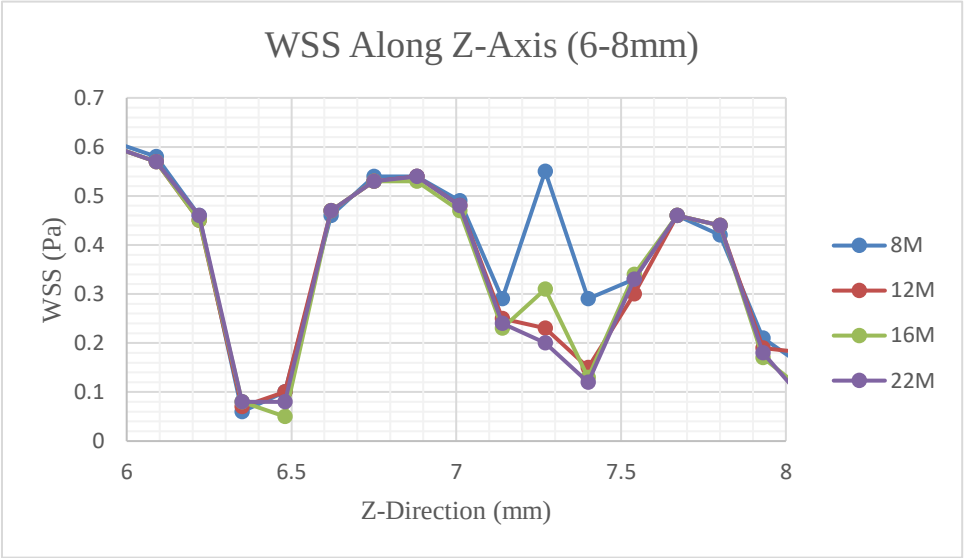

Figure 18. Comparison of various meshes for WSS

3.3.2 Temporal Convergence Study

The time step selected was based on the work of Beier et al. whereby they carried out time step convergence studies to ensure temporal convergence for all CFD analyses. The Richardson extrapolation and GCI method were used to quantify the error introduced when the time step was varied for a constant mesh size. The Courant number is used to determine temporal convergence such that,

$$C = \frac{u\Delta t}{\Delta x}$$

Where u is the fluid speed, Δt is the time step and Δx is the mesh size. The Courant number calculated in ANSYS CFX is a multidimensional generalisation of this expression where mass flow into the control volume and its dimensions determines the velocity and length scale.

The Second Order Backward Euler with High Resolution advections scheme is used for the transient solution. This is an implicit solver with second order accuracy ANSYS CFX does not require the Courant number to be small for stability [51].

Beier et al. achieved temporal convergence over a constant mesh size and selected a 0.005s time step for stent analyses and a 0.008s time step for the unstented artery [21]. The cost of a smaller time step is a higher computational load. To satisfy time constraints of the project, a temporal resolution of 0.008 seconds was selected with every time step considered for analysis (90-time steps per 0.72s cycle). The transient analyses temporal set up is shown in Table 4.

Table 4. Temporal Set-up

	Transient 1	Transient 2
Total Time (s)	2.16	2.88
Time Step (s)	0.008	0.008
Initial Time (s)	0	2.16

3.4 CFD Environment

Boundary Conditions

Inlet A parabolic inlet flow was prescribed to the inlet such that:

$$U = v_{max}\left(1 - \frac{r^2}{R_{max}^2}\right)$$

Where v_{max} is the vessel centreline velocity, R_{max} is the vessel radius, and r is the distance from centre line to R_{max}. To ensure fully developed flow, the entrance length was extended by 27mm (0.06*Re* x *3mm* vessel diameter, with *Re*= 150).

Pulsatile Flow Flow rate versus time of *0-102ml/min* was applied at the inlet, adapted from Beier et al., assuming *75 beats/min*. A no-slip wall was applied to all internal surfaces.

Outlet The outlet was extended arbitrarily by *2mm* to account for any downstream disturbance. A spatially and time constant static pressure condition was prescribed at the outlet.

Numeric Model

The computations were executed using ANSYS 19.1 CFX, a commercial CFD code. The residual RMS errors were reduced to 10-5, as the methodology was adapted from Beier et al [21].

Carreau-Yasuda Non-Newtonian Fluid Model

To account for the non-Newtonian behaviour of blood the Carreau-Yasuda model can be described as,

$$\mu = \mu_{\infty} + (\frac{(\mu_0 - \mu_{\infty})}{(1+(\lambda\dot{\gamma})^a)^{\frac{1-n}{a}}} \quad (3.1)$$

Blood density was assumed to be *1060kg/m*^{3} [21].

The Navier-Stokes equations were solved (*Equations 1.1, 1.2*). The blood flow in the coronaries is laminar, characterised by smooth fluid motion with viscous forces being dominant and Reynolds number <2000. A laminar fluid model and Second order Backward Euler transient discretisation scheme was employed [21].

Transient Settings

Four consecutive cycles were simulated following an initial steady state analysis. Only the results from the fourth cycle, at *2.72s*, were used to avoid transient start up effects. The time point selected is at peak flow as seen in *Figure 19*.

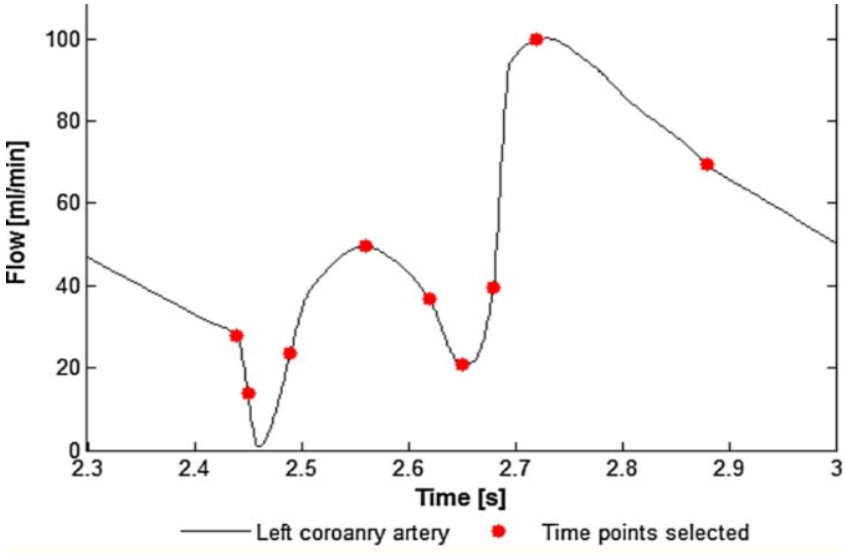

Figure 19. Left main coronary blood flow over time prescribed as the inlet boundary condition (adapted from Nichols et al.). Red circles indicate timepoints selected for transient analysis throughout the manuscript taken from the fourth simulated cardiac cycle.

A laminar numerical fluid model governed the solution of the simulated stented arterial flow, with residual targets of 10^{-4}.

Vessel Compliance and Motion

The coronaries have been simplified to be rigid and without motion as per previous studies and to spare computational cost.

3.5 Multi-Objective Optimisation

The solution methodology adopted for this study is outlined in *Figure 20*. To begin, the geometric variables to be examined are defined. A number of designs (30 in this study) are randomly distributed across the design space using the proposed variables and their defined bounds. The selection of these points is known as sampling. For each design a stent geometry is generated in CAD and then simulated for blood flow in CFD. Hemodynamic objective functions are analysed and used to construct initial surrogate models. These surrogate models are constructed by Kriging. Two separate methods are used to search these Krigs for an initial Pareto front – by NSGA and improved Hypervolume. The quality of the Krigs is improved by means of an update process. The new points are then searched again for an updated Pareto front and this process is repeated three times as per time and computational constraints.

The multi-objective optimisation problem can be mathematically formulated as follows,

$$Minimise\ Low\ WSS(CS, SD1, SD2, AT, CH, CT, NC)$$
$$Minimise\ High\ WSS(CS, SD1, SD2, AT, CH, CT, NC)$$
$$Minimise\ Low\ TAWSS(CS, SD1, SD2, AT, CH, CT, NC)$$

Such that,

$$CS = 1\ or\ 2$$
$$60mm \leq SD1 \leq 120mm$$
$$60mm \leq SD1 \leq 120mm$$
$$25° \leq SA \leq 50°$$
$$AT = 0°\ or\ 180°$$
$$0.83mm \leq CH \leq 2mm$$
$$CT = 1\ or\ 2\ or\ 3$$
$$NC = 1\ or\ 2\ or\ 3$$

There are 7 variables used to define the rectangular stent (S1,S2,SA,AT,CH,CT and NC) with the last two being categorical variables with three possibilities. Take note that 3 binary bits were each used to define two categorical variables (CT and NC) respectively.

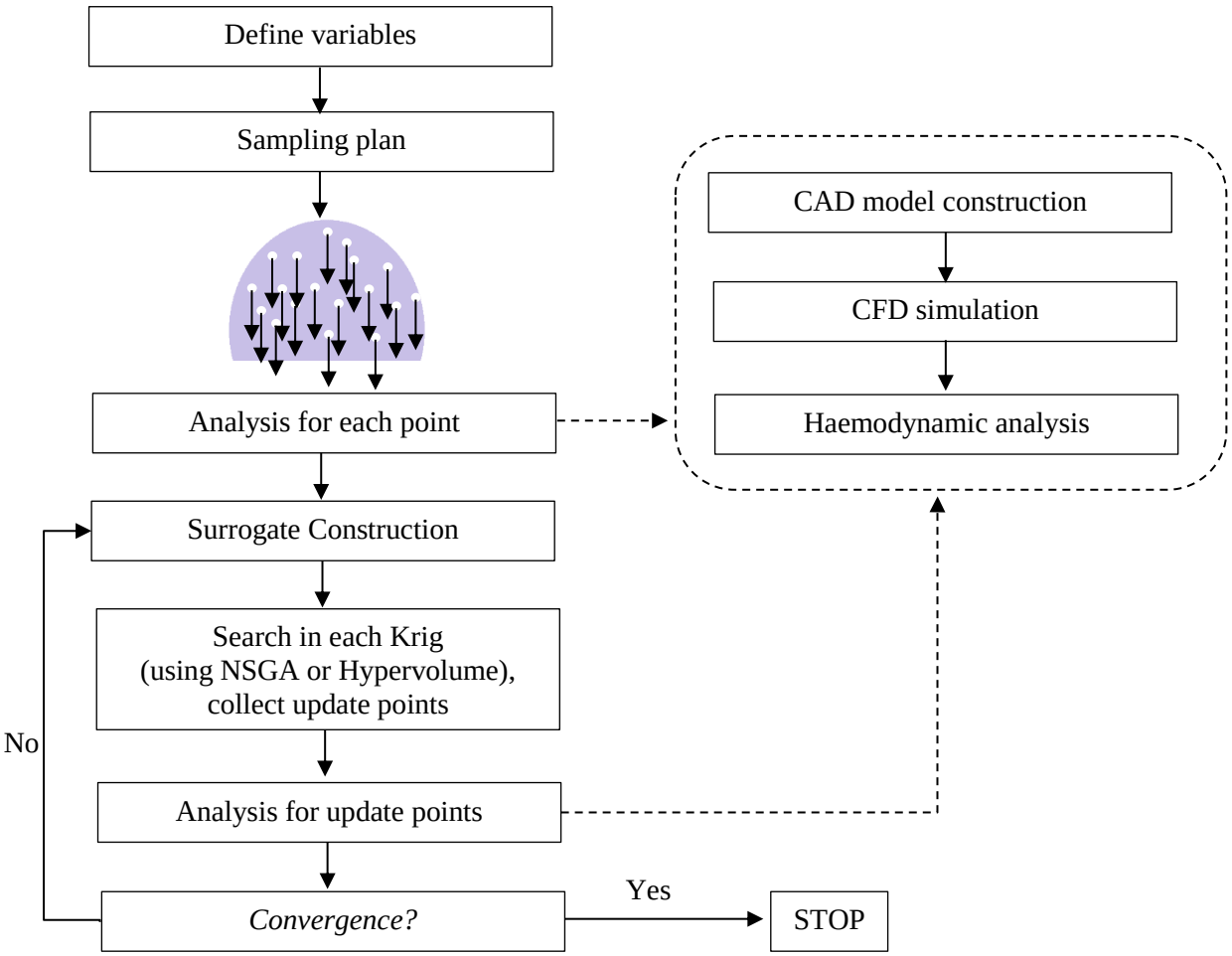

Figure 20. Flow chart detailing optimisation methodology

The lower and upper variable bounds are thus, LB= [60 60 25 0 0.83 0 0 0 0 0 0], and UB= [120 120 50 180 2.00 1 1 1 1 1 1].

As for the round stent, there are 6 variables with S2 excluded and the lower and upper variable bounds were set to LB= [60 25 0 0.83 0 0 0 0 0 0] and UB= [120 50 180 2.00 1 1 1 1 1 1].

Thus, there are 11 variables for the rectangular stent and 10 variables for the round stent configurations.

Due to the highly complex relationships of the stent design variables, a random sample is required to represent the feasible design space. To facilitate this Latin Hypercube sampling was adopted to generate 30 samples. In this sampling method points are randomly generated, and then the distance between them is maximised, effectively representing the entire design space. Examples of the generated designs can be seen in *Figure 21*. Of these 30 sample points generated, two models failed to be generated in CAD as their dimensions were physical impossibilities and outside of the feasible

design space and were thus disregarded from the results. Therefore 27 sample points were used.

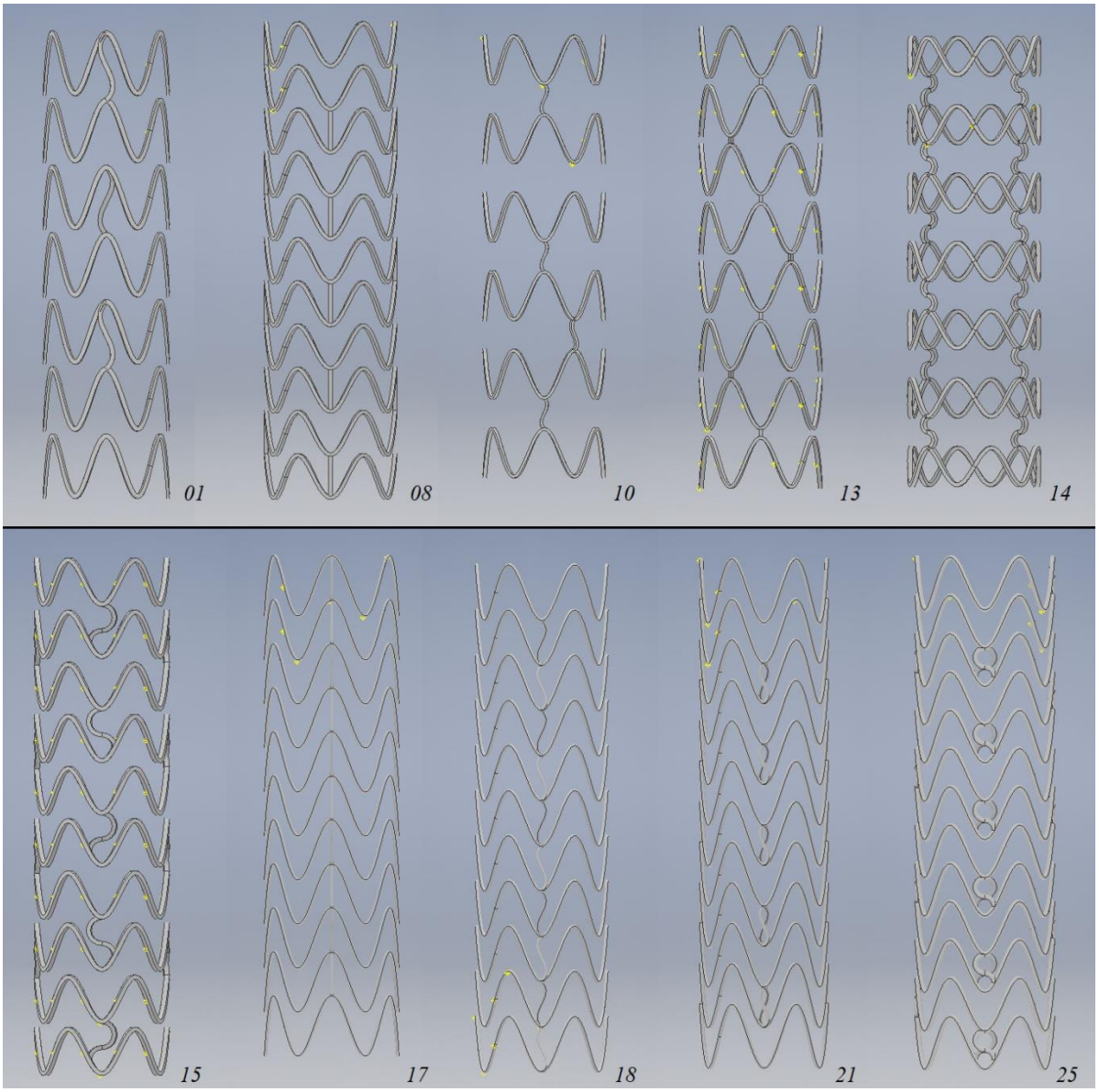

Figure 21. Sample stent designs 01, 08, 10, 13, 14, 15, 17, 18, 21 and 25. These designs also form the non-dominated solutions from the original sample of 27 designs considered.

Surrogate Model Construction and Accuracy Improvement Methods

Two surrogate optimisation methods are used in order to converge on the Pareto-optimal front and compare their findings.

In the first approach, for each stent type and for each performance function, multiple types of surrogates, i.e. response surface method of order 1 and 2, multilayer perceptron, radial basis function network and Kriging were trained using 80% of the data. The surrogate with the minimum root mean squared error was chosen as the approximator to further refine the model. These approximators were subsequently embedded within a population based stochastic algorithm (non-dominated sorted genetic

algorithm, or NSGA, in this case) to yield a set of trade-off solutions. The process was repeated for the second stent type. The resulting non-dominated sets were combined and the design which provided the maximum improvement to the was selected for.

In the second approach, Kriging models were built for each performance function and for each stent type. With these, expected hypervolume maximisation was carried out to identify the best design of each concept. Hypervolume is defined as the volume enclosed by the current non-dominated solutions and the defined reference point for the hypervolume calculation. Among the best designs identified, the one which contributed to the highest improvement to the hypervolume was selected for evaluation.

Both the approaches for surrogate modelling and the optimisation code used in this study were developed by Dr. Ray Tapabrata at UNSW Canberra.

Chapter 4

Results

Using the simulation, we obtain the wall shear stress characteristics of each stented artery. Stents 7, 9 and 30 were unable to be generated thus only twenty-seven (of 30) of the original sample set were tested. Following these, four more updates were made to improve the solution. The average computational time for each stent is 72 min and 16 s, excluding meshing and pre- and post-processing. The variable allocation and respective objective outcomes for each stent of the sample set can be seen below in Table 5.

*Table 5. Result matrix for all solutions, * non-dominated solutions*

#	CS	SD1	SD2	SA	AT	CH	CT	NC	LWSS	HWSS	TAWSS
		µm	µm	°	°	mm			% area	% area	% area
01*	**Rectangular**	61	109	27.9167	0	1.6295	2	3	2.6695	0.7979	87.8160
02	**Rectangular**	63	81	43.75	180	1.7855	3	1	2.38668	0.8054	90.0182
03	**Rectangular**	69	115	36.25	180	1.3175	3	2	3.41275	0.805108	87.9141
04	**Rectangular**	75	101	41.25	0	1.7075	2	1	2.80685	0.802628	89.3019
05	**Rectangular**	77	61	49.58333333	0	1.2395	1	2	3.67001	0.800072	90.1059
06	**Rectangular**	81	113	48.75	180	1.9025	1	3	2.51093	0.805952	89.8173
07	**Rectangular**	85	65	39.58333333	0	1.3565	2	3	inf	inf	inf
08*	**Rectangular**	89	83	37.9167	0	1.0055	1	3	5.21051	0.784281	88.0278
09	**Rectangular**	91	99	28.75	180	1.1615	2	2	inf	inf	inf
10*	**Rectangular**	93	67	32.91666667	180	1.9805	2	1	3.0494	0.7976	90.0265
11	**Rectangular**	97	105	44.58333333	0	1.5125	1	3	3.77843	0.798495	88.968
12	**Rectangular**	101	91	25.41666667	180	1.7465	3	1	4.42001	0.812488	89.4527
13*	**Rectangular**	103	75	32.08333333	180	1.4735	1	1	4.6774	0.7844	89.0989
14*	**Rectangular**	109	89	42.08333333	180	1.5905	3	2	4.6634	0.7925	89.0119

15*	**Rectangular**	115	95	37.08333333	0	1.2005	3	3	6.5300	0.7764	88.0254
16	**Circular**	65	107	42.91666667	0	1.0835	1	2	1.9802	0.80183	89.9899
17*	**Circular**	67	103	29.58333333	0	0.8885	1	1	0.7731	0.8016	88.9623
18*	**Circular**	71	77	31.25	0	1.0445	2	1	0.6746	0.8015	89.0699
19	**Circular**	73	87	38.75	0	1.6685	3	1	1.62164	0.828121	90.2771
20	**Circular**	79	69	46.25	180	1.5515	2	3	1.46757	0.832464	90.1449
21*	**Circular**	83	93	27.08333333	0	0.9665	2	2	2.5650	0.8042	87.2906
22	**Circular**	87	111	30.41666667	0	1.4345	3	2	2.45342	0.803904	88.9965
23	**Circular**	95	71	45.41666667	180	1.9415	1	1	1.7992	0.924653	90.5352
24	**Circular**	99	97	47.08333333	180	1.2785	2	1	2.6636	0.83472	89.7053
25*	**Circular**	105	73	33.75	0	0.8495	3	3	4.9855	0.8280	86.9310
26	**Circular**	107	63	40.41666667	0	0.9275	3	2	4.63824	0.90236	87.8449
27	**Circular**	111	117	47.91666667	180	1.1225	2	2	3.41904	0.821188	89.1635
28	**Circular**	113	119	34.58333333	180	1.8245	3	3	2.73157	0.84754	89.1972
29	**Circular**	117	85	35.41666667	180	1.8635	1	2	2.3749	0.893292	89.6286
30	**Circular**	119	79	26.25	180	1.3955	1	3	inf	inf	inf

4.1 Initial Sample Performance: Non-Dominated Set

Among the 27 initial samples, 13 samples were rectangular configuration, while the remaining 14 were circular in cross section. The results visualised as a trade-off of objectives can be seen in Figure 22 where objective 1 is low WSS, objective 2 is high WSS and objective 3 is TAWSS.

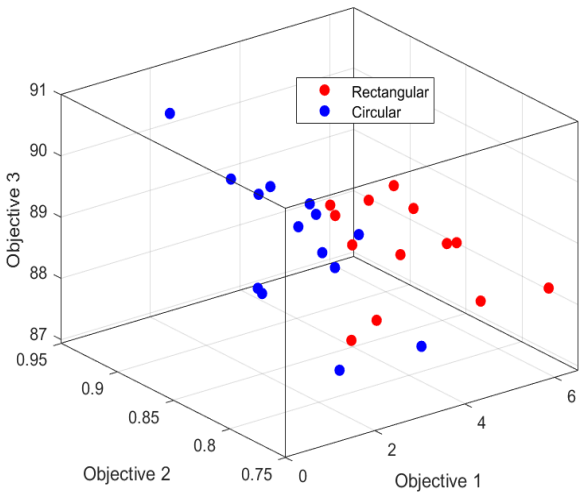

Figure 22. Multi-objective performance of initial set of 27 samples

Given the data points in bigger filled circles for rectangular and circular stent types, the set of non-

dominated solutions identified for each stent type is shown in smaller circles (*Figure 23*). Take note that is the non-dominated set created after combining the individual non-dominated set of solutions delivered for each stent type (*Figure 24*).

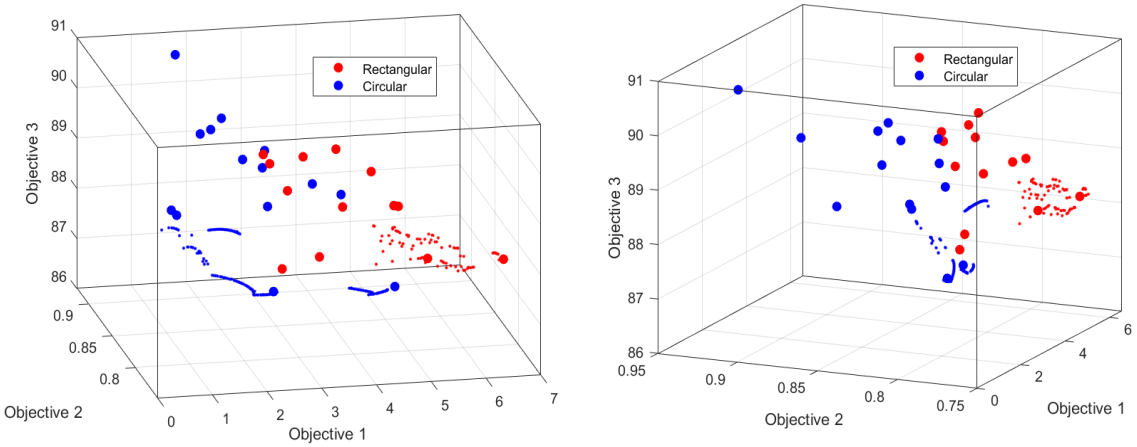

Figure 23. Two different views of the same multi-objective performance data

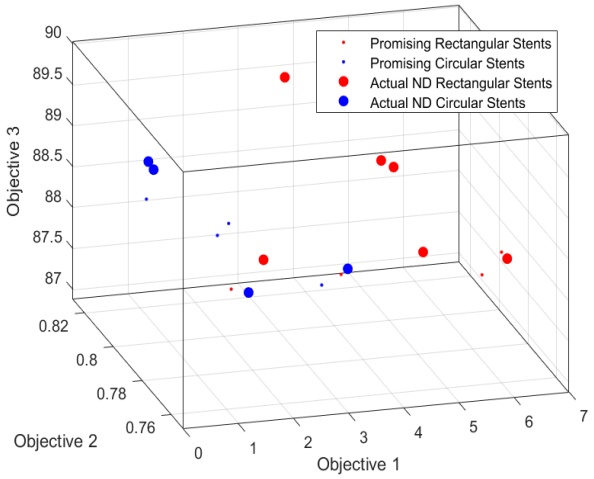

Figure 24. Truly evaluated non-dominated solutions and promising updates

Non-dominated solutions are those which, when compared to other solutions, have the most optimal values for the objectives which cannot be improved upon. There are evidently only 10 non-dominated solutions that have been truly evaluated (out of 27), below the respective results for WSS (Figure 25) and time averaged WSS (Figure 26) can be seen.

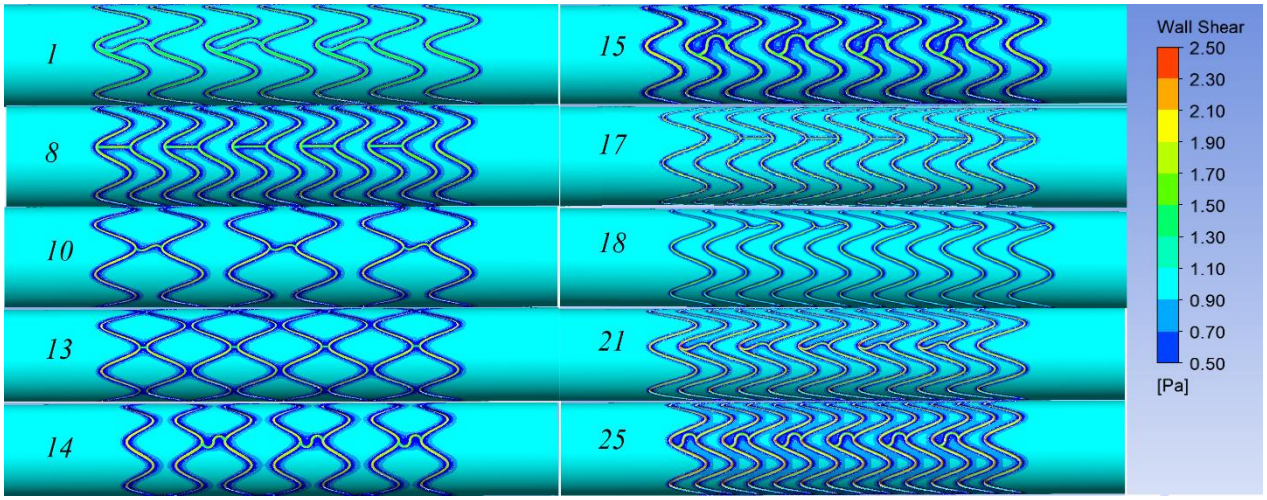

Figure 25 WSS for 10 non-dominated solutions of the initial sample set. Range shown is the idealised range, Low WSS is indicated by blue, <0.5Pa and high WSS is indicated by red, >2.5Pa

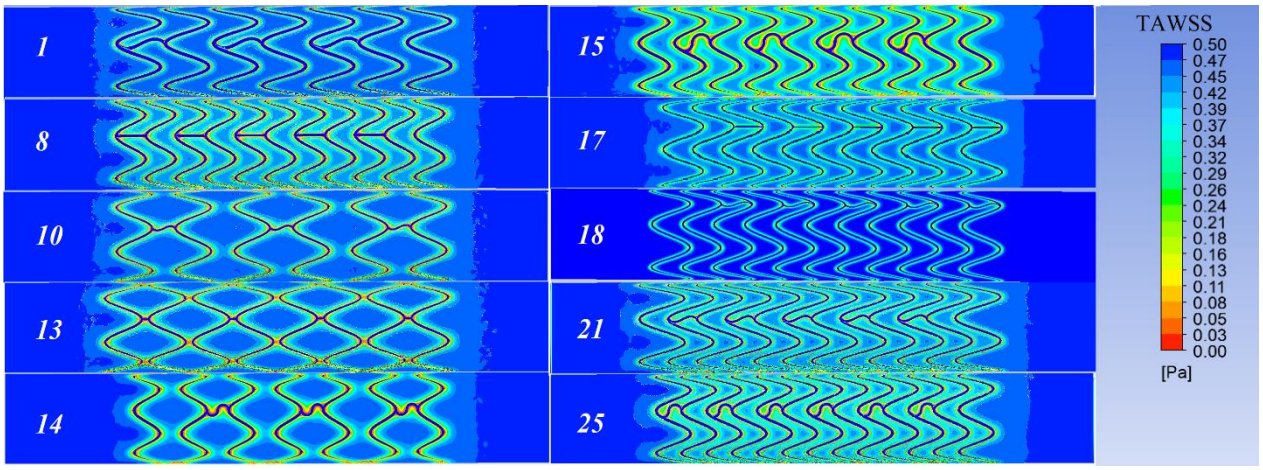

Figure 26 Time averaged WSS for 10 non-dominated solutions of the initial sample set.

4.2 NSGA Update

Three subsequent updates were made using the NGSA approach (Table 6 NSGA updates. These updates appear to be exploring the uncertainties with respect to circular stent types. The geometry of the third update was unable to be generated.

Table 6 NSGA updates

#	CS	SD1	SD2	SA	AT	CH	CT	NC	LWSS	HWSS	TAWSS
		µm	µm	°	°	mm			% area	% area	% area
N1	**Circular**	65	inf	26.25	0	1.9415	3	2	1.70854	0.922281	89.5414
N2	**Circular**	86.0334	inf	33.744	0	1.1275	2	2	2.93514	0.827157	88.8407
N3	**Circular**	78.2426	inf	26.25	0	0.8495	2	2	na	na	na

4.3 Expected Hypervolume Update

The sampling locations of the EHVI updates are seen in *Figure 27*. In the first sample location identified, marked with the black star [2, 65, 26.25, 0, 1.9415, 3, 2] (CS, SD1, SD2, SA, AT, CH, CT, NC) the maximum expected hypervolume improvement is computed in normalised performance space (higher is better). The predicted performance of this solution is [0.6192, 0.7515, 89.2093] (LWSS, HWSS, TAWSS). Upon actual evaluation, the performance is [1.70854, 0.922281, 89.5414] which indicates significant approximation error in objective 1 and objective 2.

In the second iteration of the process conducted using the previous approach and solution to update the model, the process resulted in the new sampling location as [2, 86.0334, 33.744, 0, 1.1275, 2, 2] with predicted performance of [2.6260, 0.7706, 87.6278]. Upon actual evaluation, the performance was found to be [2.93514, 0.827157, 88.8407]. The prediction accuracy in the vicinity of this solution seems to be appropriate at this stage and further iterations would be required to identify the preferred solution using this approach.

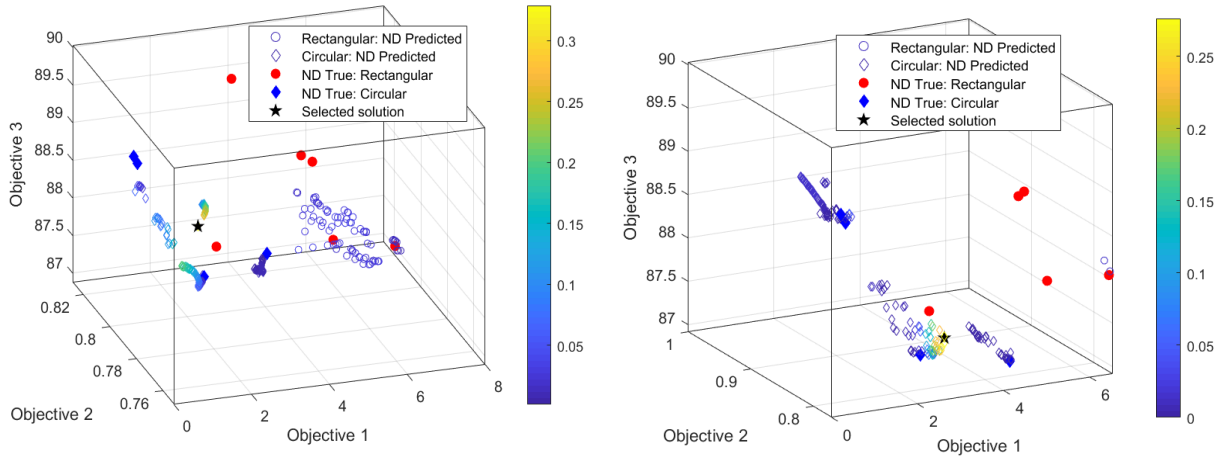

Figure 27. Expected hypervolume improvement solutions, left - solution 1, right, solution 2

Chapter 5

Discussion

Rates of stent restenosis are known to vary with stent design geometry. The relationship between the many design variables on the hemodynamic environment is complex. To derive optimal solutions for realistic applications, the performance is largely dependent on the accuracy of the underlying approximation models, which becomes increasingly challenging with an increase in the number of variables and nonlinearity of the functions. This investigation ambitiously endeavoured to consider eight crucial geometric variables for three objective outcomes. The results of this investigation are quite preliminary, an optimal set of solutions is expected with further improvement iterations. Notably, initial results have agreed with previous findings in the area. Initial design improvement has revealed several areas requiring the attention of further investigation.

There are evidently only 10 non-dominated solutions that have been truly evaluated (out of 27). Notably, these designs do not identically replicate any known commercial designs and represent potential improvements based solely on the design variables considered. However, whilst the approach has identified potential regions, it's still very sparse. Nonetheless, these identified solutions had enormous variation in all geometric variables, highlighting their complexity in manipulating blood flow. More new sampling locations are required to improve the solution.

These results confirm and extend previous findings in the area.

- High WSS values were present along the face of the strut and the lowest WSS values were localised to areas adjacent to the stent struts. This is expected as the blood flow is disrupted by the protrusion of the strut causing minor flow separation and a zone of low WSS immediately adjacent to the strut.
- Large areas of low WSS surround connectors of geometry oriented to be crossflow, most

significantly S-shaped connectors. These connectors are less stream-lined compared to *straight* and *spline* style connectors, causing disruption to the flow and over the same length increase the stent-to-vessel area. Thus, the connector shape and pattern are likely influential in design improvement.

- There appears to be a mitigating effect of cell height versus strut thickness. From qualitative analysis of the 10 non-dominated solutions it appears that increasing cell height offsets increasing strut thickness (*Figure 26*). Quantitatively there is a downward trend when comparing the area low TAWSS and cell height to average strut dimensions (*Figure 28*). Significantly, when cell height is increased relative to the average strut dimension the area of low TAWSS is minimised as desired. The significant variation in other variables, SA, AT, CT, NC may explain deviation from the trendline as they also influence the TAWSS. It should also be noted that the TAWSS analysis of stent 18 may need to be re-examined as the TAWSS is unexpectedly high between rings.

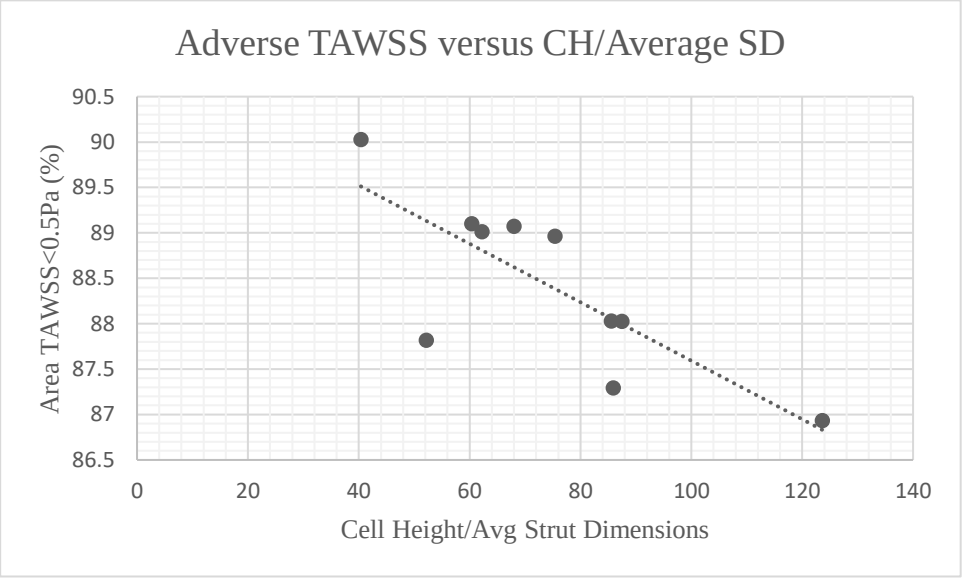

Figure 28. Adverse TAWSS (%ge area) versus cell height/average stent dimensions, ideally low TAWSS is minimised.

The range of strut dimensions, strut angle and cell height in the non-dominated solutions can be seen in *Figure 29*. The strut dimensions and cell heights observed span the plausible values with no clear indication of a more optimal range at this stage. Interestingly, the strut angles strongly cluster within the 27-42° range which is outside of the range suggested by Gundert et al. of 38.5-46°. This is likely due to the different base ring designs and stent diameters used, as these factors largely influence the 'ideal' range for *SA*. It may be capricious to suggest this range is the optimal given the uncertainty in the circular stents' non-dominated solutions. It should be understood that these results are preliminary

and design improvement iterations will likely further refine the ranges for these variables.

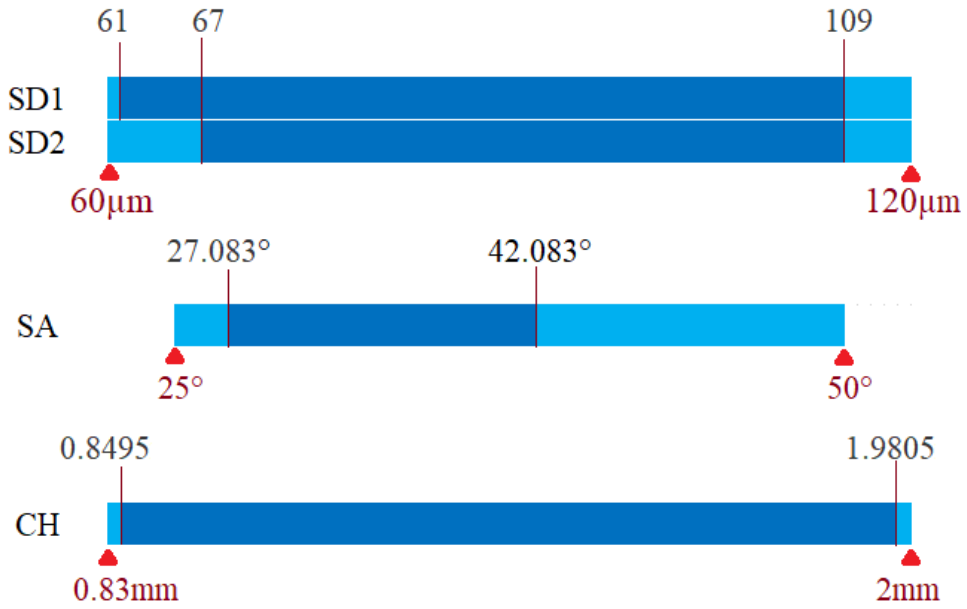

Figure 29. Non-dominated solutions' range of design variables

One can observe that potential regions of design improvement have been identified (*Figure 23)*. Interestingly, for the circular stent there seems to be disconnected segments in the non-dominated front, while for the rectangular stent, there seems to be a distribution of points that contribute to the overall non-dominated set. This could suggest a complex interplay of geometric variables and a trade-off of objectives for the circular-stent. The data from the rectangular and circular stent were combined for the overall non-dominated solutions.

The two NSGA updates concerned circular stent types to refine data on the circular designs' non-dominated solutions, mainly for *NC* and *SA*. The two subsequent sampling locations determined by EHVI also seemed to focus on these poorly explored regions for the circular stent design. Thus, both the NSGA and EHVI updates would not yet be deemed globally 'improved solutions', rather further refinement of the poorly explored regions. It would be expected that a total of eighty updates (ten times the eight variables) would be required for a thoroughly optimal solution. Nonetheless, the two updating processes show promise in refining the non-dominated solutions and Pareto front.

The time discretisation could be further improved with reduced time steps provided there is adequate computational budget. The CFL condition expresses the distance that any information travels during the time step length within the mesh against the distance between mesh elements. It would be

recommended to reduce the time step further in order to likely capture fluctuations in the transient flow should computational budget permit.

Several other WSS objectives could have been incorporated into this study to characterise the hemodynamic performance of the stent such as WSS gradient and peak WSS. While WSS gradient is a useful objective for CFD studies conducted in idealised vessels, its omission is with respect to the difficulty of interpreting these results when applied to realistic patient specific CFD simulations. The curvature of the vessel and small local geometric heterogeneities can conceal the influence of stent attributes. Peak WSS has been associated with platelet activation making it of concern for patient outcomes, however some reports have suggested that some vessels may in fact remodel to peak WSS [52]. Irrespective of the WSS objectives selected, it is important to note that the contribution of each will remain only speculative until further studies strengthen the link between these outcomes to mechanisms of stent failure. Nonetheless, the method in this study could be expanded to many more objectives in future research.

Importantly, the concept of a singular 'ideal' design is rather unreasonable given the wide variation in lesion geometry, morphology and other patient variability. To truly evaluate an 'ideal' stent design a more logical approach, though drastically more challenging in terms of computational resource, technical knowledge and practicality is attempting patient-specific optimisation using magnetic resonance imaging to better understand the geometry of lesions and morphology of the patient's vessel. Some of the findings may not be directly translatable into clinical practice, for example luminal protrusion control would be incredibly difficult to control during a routine surgical intervention. The stents examined in this investigation were implanted into a simplified environment, and thus do not account for patient-specific geometry which could further influence the hemodynamic environment.

This investigation does however present trends which can be appreciated in the context of several agreeing studies. By considering a simple, straight and rigid tube geometry the relationship of crucial geometric design variables can be better understood before being increasingly masked by the influence of vessel curvature. The optimisation method developed in this study was for the purpose of understanding how various stent geometric variables influence the hemodynamic environment. With some variation in analyses method the same parameterised CAD design could be used for improving other key objectives such as structural stability, flexibility, drug dispersion etc. for a more thorough stent investigation.

Conclusion

In conclusion, it is apparent that all eight design variables influence the hemodynamic performance of stents. However, the surplus of variables and objectives considered inherently adds complexity to the investigation. Initial results found 10 non-dominated solutions of 27 designs analysed. These solutions confirmed previous findings related to the influence of cell height, strut thickness, intra-strut angle and connector geometry on the hemodynamic environment. This is evidently an effective methodology to test different stent designs and it has the potential to reveal meaningful insights regarding optimal stent design. In the future, the methods could be extended to a wide array of objective functions and may ultimately help to identify ideal stent designs with minimum clinical risk and improved patient outcomes. Preliminary design improvement is exploring regions of uncertainty, investigations will continue, and it is expected optimal convergence on the Pareto front can be achieved within another 80 design improvement iterations.

Bibliography

[1] V. T. Turitto, "Blood viscosity, mass transport, and thrombogenesis," (in eng), *Prog Hemost Thromb*, vol. 6, pp. 139-177, 1982 1982.

[2] G. Lewis, "Materials, fluid dynamics, and solid mechanics aspects of coronary artery stents: A state-of-the-art review," vol. 86B, no. 2, pp. 569-590, 2008.

[3] S. Yusuf *et al.*, "Effect of potentially modifiable risk factors associated with myocardial infarction in 52 countries (the INTERHEART study): case-control study," *The Lancet*, vol. 364, no. 9438, pp. 937-952, 2004/09/11/ 2004.

[4] AIHW, "Cardiovascular Disease Snapshot," Web Report 24 July 2018 2018. Australian Institute of Health and Welfare

[5] Unknown. (May 5). *Balloon Angioplasty/ Stent Deployment* [Online]. Available: https://www.pinterest.com.au/ausne/.

[6] J. Butany, K. Carmichael, S. W. Leong, and M. J. Collins, "Coronary artery stents: identification and evaluation," *Journal of Clinical Pathology*, vol. 58, no. 8, pp. 795-804, 12/14/accepted 2005.

[7] U. Sigwart, J. Puel, V. Mirkovitch, F. Joffre, and L. Kappenberger, "Intravascular stents to prevent occlusion and restenosis after transluminal angioplasty," (in eng), *The New England journal of medicine*, vol. 316, no. 12, pp. 701-6, Mar 19 1987.

[8] T. Higo *et al.*, "Atherosclerotic and thrombogenic neointima formed over sirolimus drug-eluting stent: an angioscopic study," vol. 2, no. 5, pp. 616-624, 2009.

[9] S.-J. Park, S.-J. Kang, R. Virmani, M. Nakano, and Y. J. J. o. t. A. C. o. C. Ueda, "In-stent neoatherosclerosis: a final common pathway of late stent failure," vol. 59, no. 23, pp. 2051-2057, 2012.

[10] A. Kastrati *et al.*, "Restenosis after coronary placement of various stent types," (in eng), *The American journal of cardiology*, vol. 87, no. 1, pp. 34-9, Jan 1 2001.

[11] Autodesk, "Overview COmputational Fluid Dynamics Software," ed, 2015.

[12] J. Mejia, B. Ruzzeh, R. Mongrain, R. Leask, and O. F. J. B. e. o. Bertrand, "Evaluation of the effect of stent strut profile on shear stress distribution using statistical moments," vol. 8, no. 1, p. 8, 2009.

[13] S. Pant, N. W. Bressloff, A. I. Forrester, and N. J. A. o. b. e. Curzen, "The influence of strut-connectors in stented vessels: a comparison of pulsatile flow through five coronary stents," vol. 38, no. 5, pp. 1893-1907, 2010.

[14] T. J. Gundert, A. L. Marsden, W. Yang, D. S. Marks, and J. F. LaDisa, Jr., "Identification of hemodynamically optimal coronary stent designs based on vessel caliber," (in eng), *IEEE Trans Biomed Eng*, vol. 59, no. 7, pp. 1992-2002, Jul 2012.

[15] H.-M. Hsiao, Y.-H. Chiu, K.-H. Lee, and C.-H. Lin, "Computational modeling of effects of intravascular stent design on key mechanical and hemodynamic behavior," *Computer-Aided Design*, vol. 44, no. 8, pp. 757-765, 2012.

[16] J. M. Jiménez and P. F. J. A. o. b. e. Davies, "Hemodynamically driven stent strut design," vol. 37, no. 8, pp. 1483-1494, 2009.

[17] N. K. Putra, P. S. Palar, H. Anzai, K. Shimoyama, and M. Ohta, "Comparative Study Between Different Strut's Cross Section Shape on Minimizing Low Wall Shear Stress Along Stent Vicinity via Surrogate-Based Optimization," in *World Congress of Structural and Multidisciplinary Optimisation*, 2017: Springer, pp. 2097-2109.

[18] Y. Jiang, J. Zhang, and W. J. C. J. o. M. E. Zhao, "Influence of strut cross-section of stents on local hemodynamics in stented arteries," vol. 29, no. 3, pp. 624-632, 2016.

[19] E. K. Poon *et al.*, "Numerical investigations of the haemodynamic changes associated with stent malapposition in an idealised coronary artery," (in eng), *J Biomech,* vol. 47, no. 12, pp. 2843-51, Sep 22 2014.

[20] N. K. Putra, P. S. Palar, H. Anzai, K. Shimoyama, and M. Ohta, "Stent design optimization based on kriging surrogate model under deformed vessel wall: Pulsatile inlet flow," in *2017 5th International Conference on Instrumentation, Control, and Automation (ICA)*, 2017, pp. 172-176.

[21] S. Beier *et al.*, "Hemodynamics in Idealized Stented Coronary Arteries: Important Stent Design Considerations," *Annals of Biomedical Engineering*, journal article vol. 44, no. 2, pp. 315-329, February 01 2016.

[22] J. LaDisa, L. E Olson, D. Hettrick, D. Warltier, J. Kersten, and P. S Pagel, *Axial stent strut angle influences wall shear stress after stent implantation: Analysis using 3D computational fluid dynamics models of stent foreshortening*. 2005, p. 59.

[23] T. J. Gundert, A. L. Marsden, W. Yang, and J. F. J. J. o. b. e. LaDisa, "Optimization of cardiovascular stent design using computational fluid dynamics," vol. 134, no. 1, p. 011002, 2012.

[24] T. J. Gundert, A. L. Marsden, W. Yang, and J. F. LaDisa, Jr., "Optimization of cardiovascular stent design using computational fluid dynamics," (in eng), *J Biomech Eng,* vol. 134, no. 1, p. 011002, Jan 2012.

[25] N. K. Putra, P. S. Palar, H. Anzai, K. Shimoyama, and M. Ohta, "Multiobjective design optimization of stent geometry with wall deformation for triangular and rectangular struts," (in eng), *Med Biol Eng Comput,* vol. 57, no. 1, pp. 15-26, Jan 2019.

[26] Y. He, N. Duraiswamy, A. O. Frank, and J. E. Moore, Jr., "Blood flow in stented arteries: a parametric comparison of strut design fs in three dimensions," (in eng), *J Biomech Eng,* vol. 127, no. 4, pp. 637-47, Aug 2005.

[27] S. Pant, G. Limbert, N. P. Curzen, and N. W. Bressloff, "Multiobjective design optimisation of coronary stents," (in eng), *Biomaterials,* vol. 32, no. 31, pp. 7755-73, Nov 2011.

[28] W. R. Milnor, "Hemodynamics," *Cardiac dynamics*, 1989.

[29] T. J. Gundert, R. J. Dholakia, D. McMahon, and J. F. LaDisa, "Computational fluid dynamics evaluation of equivalency in hemodynamic alterations between Driver, Integrity, and similar stents implanted into an idealized coronary artery," *Journal of Medical Devices,* vol. 7, no. 1, p. 011004, 2013.

[30] S. Pant, N. W. Bressloff, A. I. Forrester, and N. Curzen, "The influence of strut-connectors in stented vessels: a comparison of pulsatile flow through five coronary stents," (in eng), *Ann Biomed Eng,* vol. 38, no. 5, pp. 1893-907, May 2010.

[31] N. Duraiswamy, R. T. Schoephoerster, and J. E. Moore, "Comparison of near-wall hemodynamic parameters in stented artery models," *Journal of biomechanical engineering,* vol. 131, no. 6, p. 061006, 2009.

[32] J. M. Jiménez and P. F. Davies, "Hemodynamically driven stent strut design," *Annals of biomedical engineering,* vol. 37, no. 8, pp. 1483-1494, 2009.

[33] R. Balossino, F. Gervaso, F. Migliavacca, and G. Dubini, "Effects of different stent designs on local hemodynamics in stented arteries," *Journal of biomechanics,* vol. 41, no. 5, pp. 1053-1061, 2008.

[34] J. F. LaDisa Jr *et al.*, "Stent design properties and deployment ratio influence indexes of wall shear stress: a three-dimensional computational fluid dynamics investigation within a normal artery," *Journal of Applied Physiology,* vol. 97, no. 1, pp. 424-430, 2004.

[35] S. Tammareddi, G. Sun, and Q. Li, "Multiobjective robust optimization of coronary stents," *Materials & Design,* vol. 90, pp. 682-692, 2016/01/15/ 2016.

[36] A. G. van der Giessen *et al.*, "3D fusion of intravascular ultrasound and coronary computed tomography for in-vivo wall shear stress analysis: a feasibility study," *The international journal of cardiovascular imaging,* vol. 26, no. 7, pp. 781-796, 2010.

[37] C. Chiastra, F. Migliavacca, M. Á. Martínez, and M. Malvè, "On the necessity of modelling fluid–structure interaction for stented coronary arteries," *Journal of the Mechanical Behavior*

of Biomedical Materials, vol. 34, pp. 217-230, 2014/06/01/ 2014.
[38] A. Razavi, E. Shirani, and M. R. Sadeghi, "Numerical simulation of blood pulsatile flow in a stenosed carotid artery using different rheological models," (in eng), *J Biomech*, vol. 44, no. 11, pp. 2021-30, Jul 28 2011.
[39] M. F. O'Rourke and W. Nichols, *McDonald's blood flow in arteries: theoretical, experimental and clinical principles*. Hodder Arnold, 2005.
[40] J. V. Soulis *et al.*, "Spatial and phasic oscillation of non-Newtonian wall shear stress in human left coronary artery bifurcation: an insight to atherogenesis," *Coronary artery disease*, vol. 17, no. 4, pp. 351-358, 2006.
[41] R. Torii *et al.*, "Fluid–structure interaction analysis of a patient-specific right coronary artery with physiological velocity and pressure waveforms," *Communications in Numerical Methods in Engineering*, vol. 25, no. 5, pp. 565-580, 2009.
[42] J. A. Grogan, S. B. Leen, and P. E. McHugh, "Optimizing the design of a bioabsorbable metal stent using computer simulation methods," (in eng), *Biomaterials*, vol. 34, no. 33, pp. 8049-60, Nov 2013.
[43] H. Li, T. Qiu, B. Zhu, J. Wu, and X. Wang, "Design optimization of coronary stent based on finite element models," (in eng), *ScientificWorldJournal*, vol. 2013, p. 630243, 2013.
[44] M. A. Atherton and R. A. Bates, "Robust optimization of cardiovascular stents: a comparison of methods," *Engineering Optimization*, vol. 36, no. 2, pp. 207-217, 2004/04/02 2004.
[45] M. De Beule *et al.*, "Virtual optimization of self-expandable braided wire stents," *Medical Engineering & Physics*, vol. 31, no. 4, pp. 448-453, 2009/05/01/ 2009.
[46] A. Amirjani, M. Yousefi, and M. Cheshmaroo, "Parametrical optimization of stent design; a numerical-based approach," *Computational Materials Science*, vol. 90, pp. 210-220, 2014/07/01/ 2014.
[47] F. Bozsak *et al.*, "Optimization of Drug Delivery by Drug-Eluting Stents," (in eng), *PLoS One*, vol. 10, no. 6, p. e0130182, 2015.
[48] A. Blouza, L. Dumas, and I. M'Baye, "Multiobjective optimization of a stent in a fluid-structure context," in *Proceedings of the 10th annual conference companion on Genetic and evolutionary computation*, 2008: ACM, pp. 2055-2060.
[49] R. Clune, D. Kelliher, J. C. Robinson, and J. S. Campbell, "NURBS modeling and structural shape optimization of cardiovascular stents," *Structural and Multidisciplinary Optimization*, vol. 50, no. 1, pp. 159-168, 2014.
[50] K. Shimoyama, S. Jeong, and S. Obayashi, "Kriging-surrogate-based optimization considering expected hypervolume improvement in non-constrained many-objective test problems," in *2013 IEEE Congress on Evolutionary Computation*, 2013, pp. 658-665.
[51] SHARCNET. (2019, 10 May). *Variable Names* [Online]. Available: https://www.sharcnet.ca/Software/Ansys/16.2.3/en-us/help/cfx_thry/i1298716.html#cfxBasiVariCour.
[52] K. N. Bharadwaj, C. Spitz, A. Shekhar, H. C. Yalcin, and J. T. Butcher, "Computational Fluid Dynamics of Developing Avian Outflow Tract Heart Valves," *Annals of Biomedical Engineering*, journal article vol. 40, no. 10, pp. 2212-2227, October 01 2012.